Cooperative Research Centre for
Landscape Environments
and Mineral Exploration

OPEN FILE
REPORT
SERIES

SUPERGENE GOLD DISPERSION AT THE ARGO AND APOLLO DEPOSITS, WESTERN AUSTRALIA

A.F. Britt and D.J. Gray

CRC LEME OPEN FILE REPORT 219

April 2007

(CRC LEME Restricted Report 114R / E&M Report 639R, August 1999)

SUPERGENE GOLD DISPERSION AT THE ARGO AND APOLLO DEPOSITS, WESTERN AUSTRALIA

A.F. Britt and D.J. Gray

CRC LEME OPEN FILE REPORT 219

April 2007

(CRC LEME Restricted Report 114R / E&M Report 639R, August 1999)

CRC LEME is an unincorporated joint venture between CSIRO-Exploration & Mining, and Land & Water, The Australian National University, Curtin University of Technology, University of Adelaide, Geoscience Australia, Primary Industries and Resources SA, NSW Department of Primary Industries and Minerals Council of Australia.

Headquarters: CRC LEME c/o CSIRO Exploration and Mining, PO Box 1130, Bentley WA 6102, Australia

PREFACE

The principal objective of CRC LEME-AMIRA Project 504, *Supergene mobilization of gold and other elements in the Yilgarn Craton*, is to determine the mechanisms of supergene/secondary depletion, enrichment and dispersion of Au and other elements, so as to improve selection of drilling targets and further optimize interpretation of geochemical data.

Argo and Apollo are two closely adjoining Au deposits close to Lake Lefroy, in the Kambalda region. This region is similar to the Kalgoorlie area in having saline/acidic groundwaters and major influences from palaeochannel systems. However, it differs in that it is lower in the landscape, with groundwaters trending even more hypersaline than around Kalgoorlie, and with the presence of lignite within the palaeochannel sediments. The Argo deposit is overlain by up to 60 m of palaeochannel sediments, with mineralization at the unconformity between *in situ* and transported regolith and in saprolite. This allows investigation of the distribution of Au within both *in situ* and transported materials. In contrast, most of the Apollo deposit is away from the palaeochannel area, thus allowing investigation of the supergene redistribution of Au in residual regolith.

Thus, these two deposits offer an ideal area to investigate differing modes of Au redistribution in transported and in situ regolith in the Kambalda/Lefroy region, and this study fits well within the objectives of the Project.

D.J. Gray
Project Leader
August 1999

ABSTRACT

This report discusses the three-dimensional stratigraphy and Au geochemistry of the Argo and Apollo Au deposits. Using the highly consistent WMC logging, the residual profile at the Argo and Apollo Au deposits could be divided into bedrock, saprock, saprolite, residual clay and ferruginous residual clay whereas the overlying sediments were split into basal gravels and sands, lignite, spongolite and lake clays between these units. Alluvium overlies the entire region. These units are in broad correspondence with previous studies. Gold concentrations have been calculated for each regolith unit and the variation in Au content has been displayed according to elevation or distance from unit contacts.

The three-dimensional stratigraphic modelling indicated that the weathering front is broadly deepened below the palaeochannel. In addition, there are narrow lows along the strike of the two deposits associated with two north-south shear zones. Of the major *in situ* units (saprock, saprolite and residual clay), the residual clay is generally thickest, but it, the saprolite and, sometimes, the saprock are truncated directly beneath the palaeochannel, suggesting that incision of the channel post-dates the major weathering. There is also a thin ferruginous clay unit that is mostly confined to the upland areas and hill flanks of the pre-Eocene topography.

Gold geochemistry models show the Argo and Apollo Au deposits have patchy Au concentrations greater than 1 ppm within the bedrock and are enriched in the saprock, saprolite and lower residual clay. A major Au depletion occurs above 270 - 276 mRL elevation, which is about 20 - 30 m below surface. The depletion appears to be of the order of 60 - 80% at Apollo and greater than 90% at Argo.

Within the palaeochannel sediments, the basal gravel and, to a lesser extent, the sand are strongly enriched in Au (1636 ppb and 652 ppb means, respectively). Above these horizons there is an almost smooth reduction in Au concentration going up through the palaeochannel sediments: lower lake clays (287 ppb), lignite (168 ppb), middle lake clays (133 ppb), spongolite, which is particularly low in Au, (30 ppb) and upper lake clays (100 ppb). The previously suggested association of Au with lignite in the palaeochannel is not observed, but instead appears related to position with respect to the unconformity. Mean Au concentration of 39 ppb is observed in the alluvium and is postulated to be erroneously high, due to cross-hole contamination.

TABLE OF CONTENTS

LIST OF FIGURES

LIST OF TABLES

APPENDICES

1 INTRODUCTION

1.1 OBJECTIVE

The principal objective of CRC LEME-AMIRA Project 504, *Supergene mobilization of gold and other elements in the Yilgarn Craton*, is to determine the mechanisms of supergene/secondary depletion, enrichment and dispersion of Au and other elements, so as to improve selection of drilling targets and further optimize interpretation of geochemical data.

Within this framework, this study has investigated the geochemical dispersion of Au at the Argo and Apollo Au deposits using the Mining Visualization System (MVS) program. This program is a useful tool for visualizing the three-dimensional patterns of Au distribution in the regolith and calculating degrees of depletion and enrichment.

1.2 LOCATION

The Argo and Apollo Au deposits are located approximately 28 km SE of Kambalda and 2 km east of Lake Lefroy at latitude 31° 24’ S and longitude 121° 47’ E (Figure 1). The Apollo Au deposit is about 500 m NE of Argo.

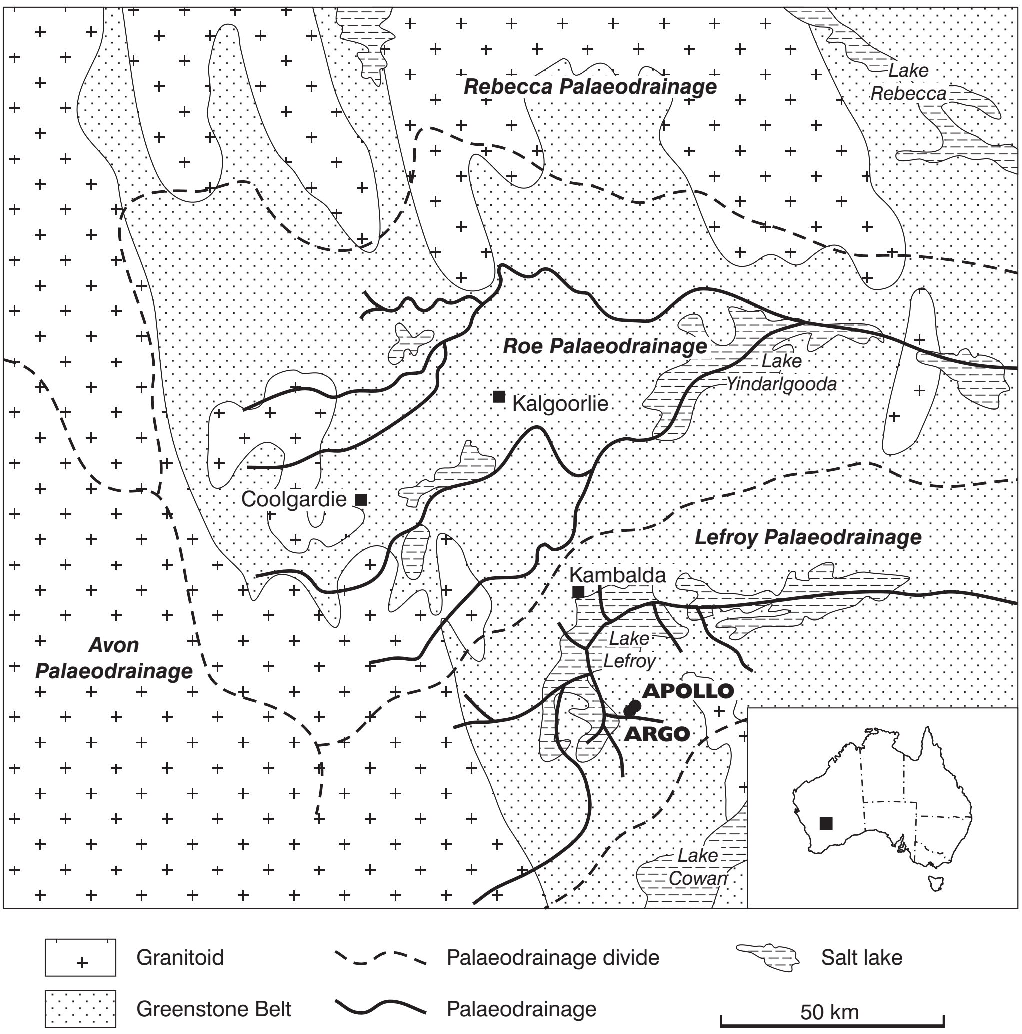

Figure 1: Location of Argo and Apollo Au deposits

1.3 CLIMATE, VEGETATION AND GEOMORPHOLOGY

(Summary taken from Butt et al., 1997).

The climate is semi-arid with unreliable average rainfall of 280 mm. Vegetation is open woodland and composed of *Eucalyptus* species, the occasional *Casuarina* (she-oak), *Eromophila* (poverty bush), bluebush and other small shrubs. A broad colluvial plain with occasional clay pans drains the Argo-Apollo area to the SW, towards Lake Lefroy, where dunes cover large areas. The landscape is typical of the floodplains bordering the salt lake regimes of the region.

In contrast, the pre-Cainozoic geomorphology of the region was quite different. The weathered Archaean basement was incised by deep river channels, with that at Argo up to 60 m deep and averaging 400 m in width (Woolrich, 1994).

1.4 GEOLOGICAL SETTING, BEDROCK AND MINERALIZATION

(Summary taken from Butt et al., 1997).

The Argo and Apollo Au deposits are located in the western limb of the St Ives Antiform, part of the Archaean Norseman-Wiluna Greenstone belt of the Yilgarn Craton. The local bedrock consists of the Paringa Basalt, the Black Flag Group and the Condensor Dolerite, all of which are metamorphosed to low grade, strike NE and dip 70-80° SW. The deposits are hosted in the Condensor Dolerite, a sill up to 400 m thick, fractionated *in situ* to four zones. There is an increase in Fe and silica content from Zone 1 to 4, and the Au mineralization tends to have an affinity with the highly siliceous and Fe-rich Zone 4. Mineralization is associated with albite alteration products within two NNE trending mylonitic shear zones of variable dip to the west.

1.5 PREVIOUS WORK

The characteristics and evolution of the stratigraphy, regolith and geomorphology of the Lefroy region and are described thoroughly by Clarke (1994a, b, c). Woolrich (1994) specifically worked on the local regolith stratigraphy at the Argo palaeochannel and studied Au grain composition and morphology in the basal sediments. More recently, Zheng et al. (1998) discussed the local stratigraphy, geomorphology and the timing of aridification and Carey and Dusci (1999) described the Lake Lefroy regolith and the Au dispersion and geochemical interpretation of some of the local Au deposits.

Lintern and Gray (1995) released a preliminary report on the Argo deposit as part of CRC LEME/AMIRA project 409, “Geochemical exploration in areas of transported overburden, Yilgarn Craton and environs, WA”. This was followed by a study on the Apollo deposit as part of the same project (Lintern et al, 1997). Several further investigations were suggested, including testing the possibility that lignite acts as a scavenger and better assessment of anomalous Au concentrations in the soil over mineralization.

2 METHODS

2.1 DATA MANIPULATION AND MODELLING

WMC Resources Ltd supplied logging and geochemical data. From this data, the major regolith divisions of bedrock, saprock, saprolite, residual clay, ferruginous residual clay, lake sediments and alluvium were recognized. Furthermore, due to the high consistency of the logging, the lignite- and spongolite-dominated horizons could be distinguished from the surrounding lake sediments. The first occurrence of spongolite recorded in an individual drill hole was defined as the top of the horizon and the lowermost occurrence as the bottom. The top and bottom of the lignite horizon were defined the same way. Note that spongolite and lignite were not necessarily recorded at every interval between the uppermost and lowermost points, hence the horizons can only be regarded as being dominantly spongolite or dominantly lignite.

Lake sediments overlying the spongolite were named "upper lake clays"; those between the spongolite and lignite were named "middle lake clays" and those beneath the lignite, "lower lake clays". These lake clays are various fluvial, near-shore marine and lacustrine facies such as sand, clay and lignitic silts. For drill holes with no spongolite, the lake clays overlying the lignite were split evenly into middle and lower lake clay units. When lignite was not recorded in the drill hole, then the sediments underlying the spongolite were split evenly into middle and lower lake clay units. When neither spongolite nor lignite were recorded, the lake clays were evenly split into upper, middle and lower units. On this basis, a total of thirteen regolith layers was established (Table 1).

Table 1: Regolith layers defined for modelling at the Argo and Apollo Au deposits.

Regolith Layer	Description
Alluvium	Sandy topsoil and calcareous clay-rich red soil
Upper Lake Clays	Hard mottled red and grey silts and clays
Spongolite	Spiculite, silts, clays and sands
Middle Lake Clays	Silty lignitic clays and some sands
Lignite	Silty clays dominated by lignite
Lower Lake Clays	Silty lignitic clays and some sands
Sand	Fluvial coarse to fine sand, dominantly quartz
Gravel	Fluvial gravels, dominantly quartz
Ferruginous Residual Clay	Ferruginous plasmic clay
Residual Clay	Plasmic clay, variably coloured, often green
Saprolite	Weathered mafic rocks, clay-rich, variably coloured, often green
Saprock	Weathered mafic rocks
Fresh Rock	Dominantly mafic rocks

The distributions of these regolith layers were modelled using Mining Visualization System (MVS; © C Tech Corporation). The program grids three-dimensional data by kriging, which is able to take into account variables such as trends and bias. The module used was KRIG_3D_GEOLOGY.

Output was manually filtered with "point" anomalies individually assessed. In general, small errors were deemed acceptable, but data resulting in large errors were disregarded, though with a bias for including data, rather than removing it and losing information. Kriging and filtering took several cycles, with less than 2% of data removed for all regolith layers.

Following this, the Au geochemistry was gridded using the KRIG_3D module.

Five areas (Figure 2) were gridded and Table 2 lists the parameters used for each area. The five areas are:

1. The Argo-Apollo region. This is the region around the Argo and Apollo deposits covered by the WMC data set. Regolith stratigraphy and Au distribution were modelled.
2. The Argo & Apollo area. This is the immediate area around the Argo and Apollo deposits. Here, the data were more dense, resulting in more accurate interpolation when kriging. Regolith stratigraphy and Au distribution were modelled.
3. The Argo deposit. As above, the data in this area were comparatively dense, allowing relatively detailed modelling. Regolith stratigraphy and Au distribution were modelled and the Au concentrations of each regolith layer were calculated.
4. The Argo channel. This small section of the palaeochannel was chosen as best for calculations of the vertical distribution of Au in the transported regolith profile.
5. Apollo deposit. This area was chosen as best for calculations of Au distribution in the regolith distant from the palaeochannel; thus the southern part of the deposit was not included.

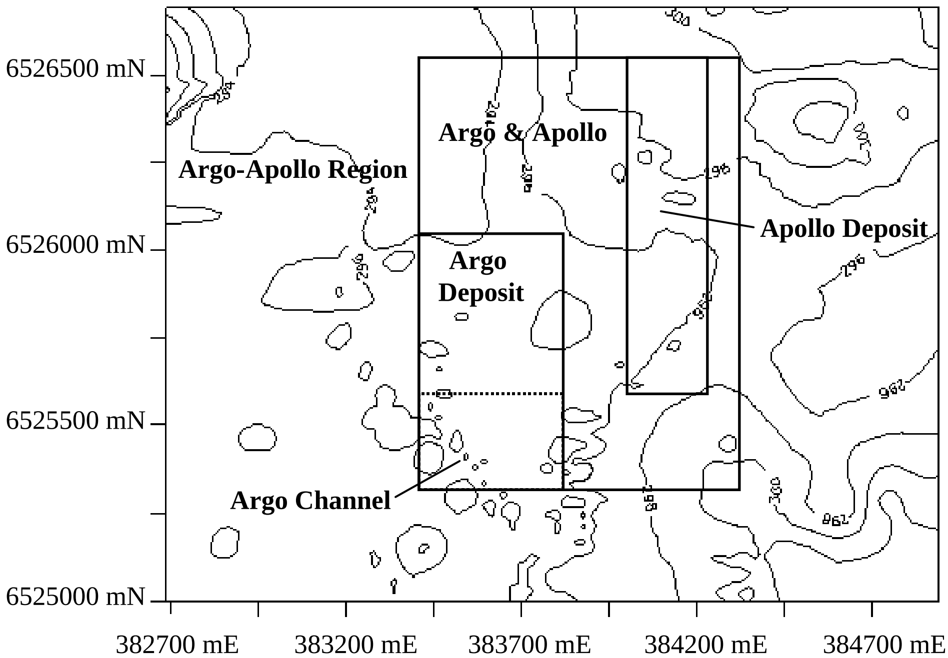

Figure 2: The five areas of the study: the Argo-Apollo region; the immediate area around the Argo and Apollo deposits; the Argo deposit; the Argo channel; and the Apollo deposit. The map shows the modern surface topography with elevation given in mRL.

The main procedures undertaken for this project were modelling the regolith stratigraphy, modelling the Au distribution in the regolith and calculating Au concentration statistics. Models of the regolith stratigraphy and Au distribution are presented diagrammatically on the enclosed CD. The Au concentration statistics are discussed in Section 5.

Table 2: Gridding parameters for the Argo-Apollo region, the Argo and Apollo deposits, the Argo deposit, the Argo channel and the Apollo deposit.

		Argo-Apollo Region	Argo-Apollo Deposits	Argo Deposit	Argo Channel	Apollo deposit
Krig_3D_Geology Parameters						
Kriging	Minimum X	382686	383400	383400	383400	384000
	Maximum X	384888	384300	383800	383800	384250
	Minimum Y	6525000	6525300	6525300	6525300	6525650
	Maximum Y	6526691	6526600	6526200	6525600	6526600
	Points	80	80	70	80	80
	X resolution	90	91	58	41	51
	Y resolution	68	131	129	31	191
	Boundary Offset	0	0	0	0	0
	Smoothing	0	0	0	0	0
	Gridding Option	Rectilinear	Rectilinear	Rectilinear	Rectilinear	Rectilinear
Krig_3D Parameters						
Kriging	Minimum X	382686	383400	383400	383400	384000
	Maximum X	384888	384300	383800	383800	384250
	Minimum Y	6525000	6525300	6525300	6525300	6525650
	Maximum Y	6526691	6526600	6526200	6525600	6526600
	Minimum Z	195	195	195	195	195
	Maximum Z	303	300	298	298	300
	Points	120	120	70	80	120
	X resolution	90	91	58	41	51
	Y resolution	68	131	129	31	191
	Z resolution	42	45	42	45	53
	Rectilinear Offset	0	0	0	0	0
	Horiz./Vert. Anisotropy	2.5	2.5	2.5	2.5	2.5
Post Processing	Clip Minimum	0	0	0	0	0
	Clip Maximum	18	20	20	20	40

2.2 REGOLITH STRATIGRAPHY

The regolith stratigraphy was modelled for the Argo-Apollo region, the area surrounding the Argo and Apollo deposits, and the Argo deposit. Three-dimensional images for Argo-Apollo area and for the Argo deposit were modelled with the 3D_PLUME module and the EXPLODE_AND_SCALE module, which allows various layers to be removed and/or exploded. Two-dimensional cross sections of the regolith stratigraphy for the Argo-Apollo region (Transects A-J, Figure 3) approximately parallel and perpendicular to the palaeochannel (e.g., Figure 13), as well as two-dimensional north-south cross sections (e.g., Figure 16), of the Argo area were modelled using the EXPLODE_AND_SCALE and SLICE modules. The colours consistently used for each layer are given in Table 3.

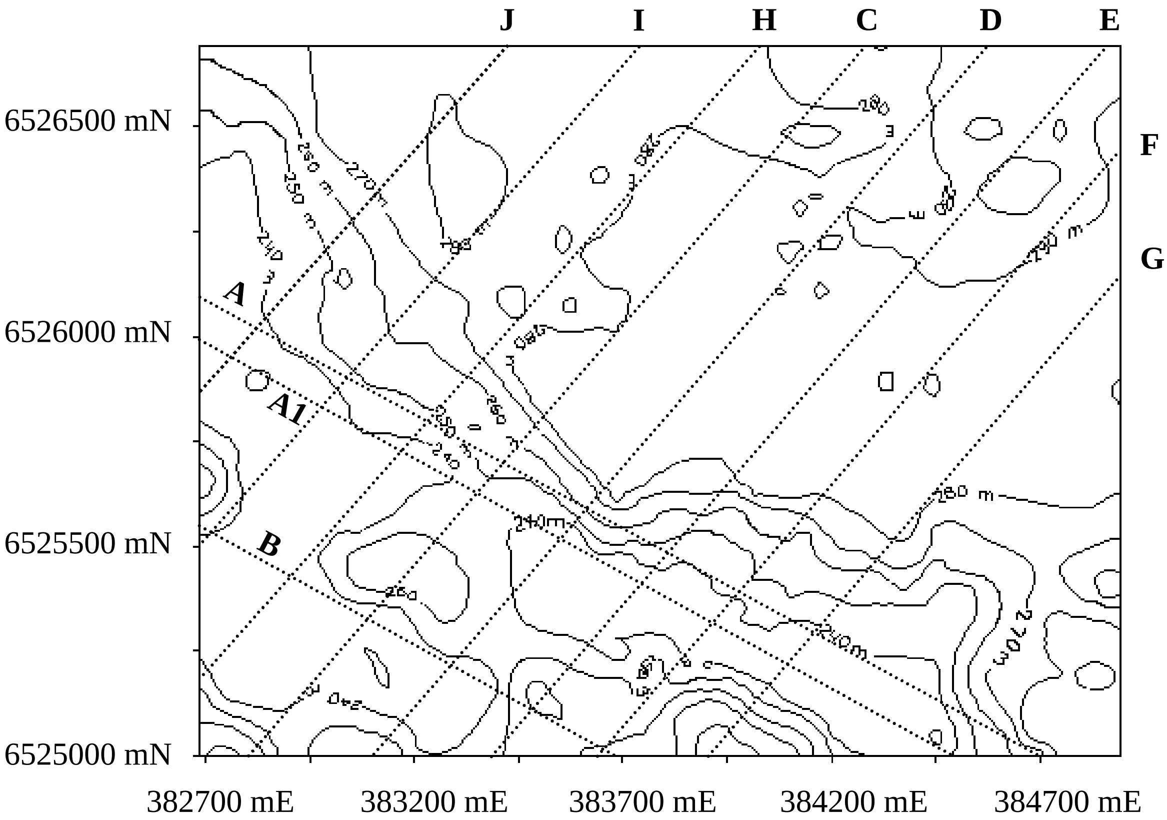

Figure 3: Transects (A-J) across the Argo-Apollo region showing the locations of the two-dimensional regolith and gold distribution cross-sections (Appendices 1.8 and 1.9, enclosed CD). The map shows the surface of the residual regolith with elevation in mRL (see Figure 11).

Table 3: Regolith layers and colours used for modelling exercises

Regolith Layer	Colour	Hue/Saturation/Value
Alluvium	Yellow	0.18/0.60/1.00
Upper Lake Clays	Purple	0.75/0.40/0.60
Spongolite	Bright Green	0.33/1.00/1.00
Middle Lake Clays	Purple	0.75/0.40/0.60
Lignite	Black	0.00/0.00/0.10
Lower Lake Clays	Purple	0.75/0.40/0.60
Sand	Yellow	0.20/1.00/1.00
Gravel	Orange	0.12/1.00/1.00
Ferruginous Residual Clay	Red	0.00/1.00/1.00
Residual Clay	Blue-Green	0.42/0.70/1.00
Saprolite	Green	0.40/1.00/1.00
Saprock	Green	0.40/1.00/1.00
Fresh Rock	Dark Green	0.45/1.00/0.40

The same colour is used for the upper, middle and lower lake clays as these are not different regolith units but lake materials surrounding the lignite and spongolite dominated horizons. The same colour is used for saprock and saprolite because logging of the saprolite/saprock transition was less consistent than for the other horizons.

2.3 GEOCHEMICAL DISTRIBUTION

Gold distributions at the interfaces between each regolith layer were modelled for the Argo-Apollo region, the area surrounding the Argo and Apollo deposits, and the Argo deposit. The regolith stratigraphy was defined with the KRIG_3D_GEOLOGY module and interfaces were selected with the GEOLOGICAL_SURFACE module. The INTERP_DATA module combined the data to create the models of Au distribution at each interface. The data was filtered so that the minimum Au value was set to 10 ppb and the maximum Au value to 1 ppm. Thus, all values of 10 ppb and lower are displayed at the low end of the colour scale (blue) and all values of 1 ppm or greater are displayed at the high end of the colour scale (red), creating a greater contrast between mineralized areas and background. Diagrams for each interface and for each area are contained on the CD in plan and oblique (three-dimensional) views (see Figure 14).

Two-dimensional cross sections of Au distribution through the regolith profile were created for the Argo-Apollo region and the Argo deposit. The EXPLODE_AND_SCALE module was used to read the regolith stratigraphy and geochemistry from an input file and to choose which regolith layers would be displayed. Two SLICE modules were used to create slices showing the Au distribution in relation to regolith stratigraphy. Slices for the Argo-Apollo region correspond with the cross-sections of regolith stratigraphy (Figure 3). Slices for the Argo deposit are north-south oriented and are more intensely spaced in the mineralized zone.

Three-dimensional models of the Au dispersion at the Argo deposit were made by creating input files which contained gridded data for each regolith layer, but only where the corresponding Au concentration was equal to or above the values of 30 ppb, 100 ppb, 300 ppb and 1 ppm Au, which range from background to mineralization. The regolith stratigraphy was displayed with the nominated Au cut-off, thus creating a three-dimensional image of Au distribution in relation to regolith stratigraphy. Diagrams for each cut-off showing the three-dimensional distribution of Au, at different angles, are contained on the CD.

2.4 GOLD CONCENTRATION CALCULATIONS

The MVS VOLUME_AND_MASS module was used to calculate volume and Au concentration for individual regolith layers. No attempt was made to model different densities for different layers. As the Au concentration data is as mass/mass rather than mass/volume, uniform density has only a minor influence on most calculations. The calculated concentrations do not compensate for leaching of mobile constituents: if half of the minerals have dissolved and been leached then Au concentration will double because of residual concentration.

In addition, by using the ISOVOLUME module, Au concentration can be calculated for slices defined either by elevation (e.g., 390-393 mRL) or distance from a regolith contact (e.g., 3-6 m above the unconformity) (Figure 4). Although this method is (arithmetically) correct, it can lead to over- or underestimations as the slices get further from the boundary in question. This is because, ultimately, the slice being analyzed is incomplete. This can be expressed as a reliability factor, which is the mass of the slice divided by the mass of an untruncated slice (Figure 4). A reliability index of 85% indicates that the slice is 15% truncated.

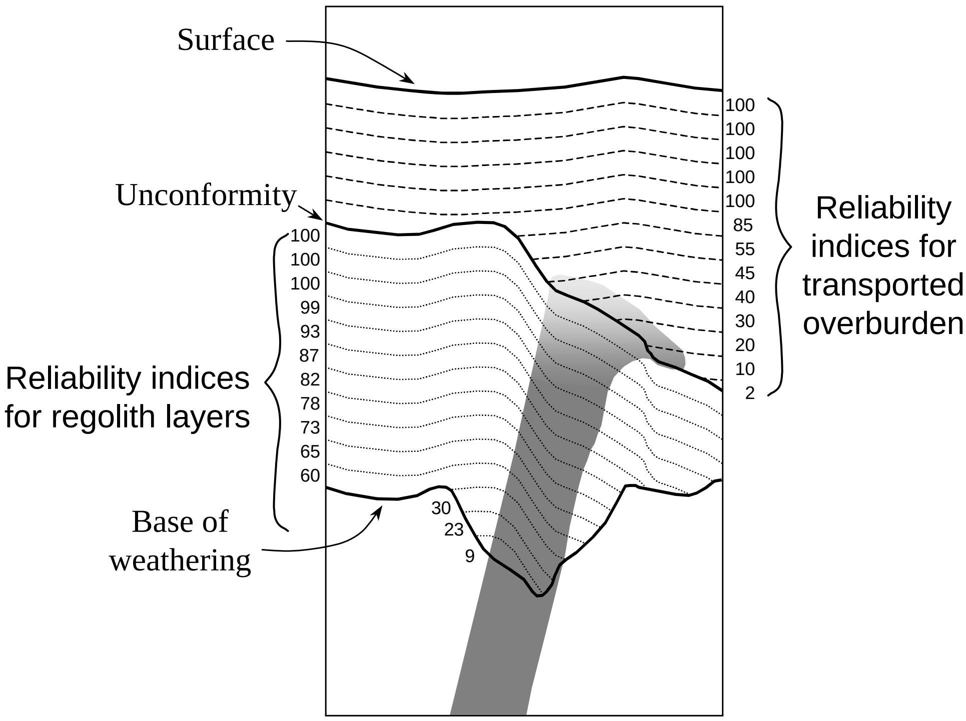

Figure 4: Diagrammatic representation of method for calculating Au concentration from slices defined for the upper surface and for the unconformity. The shaded area represents mineralization, with depletion near the top of the in situ regolith.

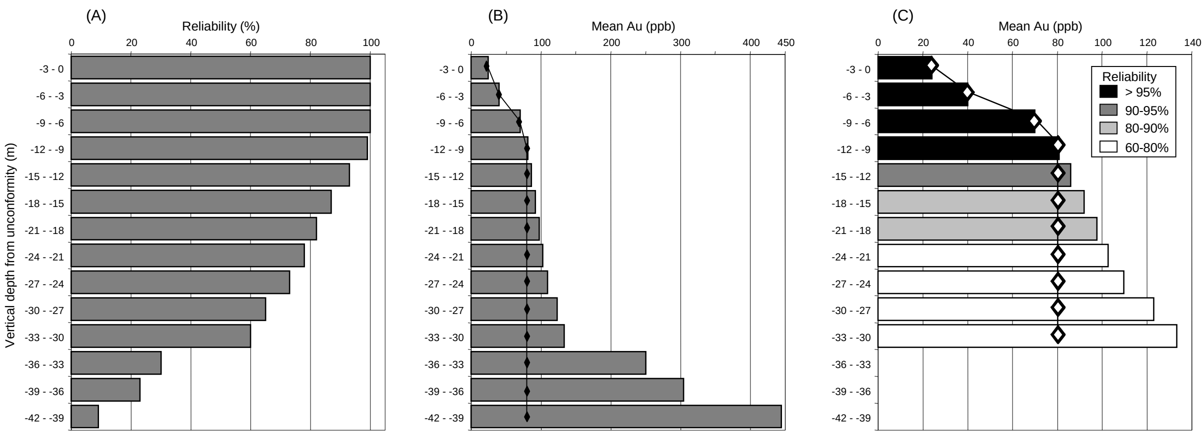

Figure 5: Calculated (a) reliability (b) unfiltered Au concentration and (c) filtered (> 60% reliability) Au concentration, colour coded to reliability, for in situ regolith. Diamonds represent expected Au concentration. Data based on situation represented in Figure 4.

As the reliability index decreases, significant errors can occur. Figure 5 shows the results of Au content measurement for each slice from the unconformity. Though the deeper slices are truncated (Figure 5a), they can still contain mineralized material, as in this example (Figure 4). Thus, a similar mass of Au is being divided by smaller and smaller masses of regolith, which leads to anomalous calculations of Au concentration (Figure 5b). In this example, the results indicate that deepest slice has up to 440 ppb Au even though the “real” Au content is invariant at 80 ppb, except for the depletion zone at the top of the *in situ* regolith.

When all the slices with reliability indices less than 60% are removed, the remaining results can be coded for reliability (Figure 5c). A much clearer picture of Au trends emerges, illustrating depletion towards the unconformity. Note that this example is for the maximum possible overestimation of Au concentration (the maximum overestimation = 100 ÷ reliability: e.g., if reliability is 60%, maximum overestimation is 1.67; if reliability is 90%, maximum overestimation is 1.11). In other cases, underestimation can occur for low reliability samples due to a truncated intersection with mineralization. In summary, samples with reliabilities less than 80% are suspect (but can still be valuable if treated with caution), whereas those with reliability less than 60% should generally not be used.

The mean Au concentration of each regolith layer was calculated for the Argo deposit. Additionally, horizontal slices, 3 m thick, were used on a small area of the Argo channel (Figure 2) to calculate the vertical changes in Au distribution in the transported part of the profile. For contrast, an area away from the palaeochannel, the northern part of the Apollo deposit (Figure 2), was chosen for Au concentration and reliability calculations using 3 m slices parallel to the pedoplasmation front (saprolite/residual clay interface), the weathering front (bedrock/saprock interface), and the unconformity (residual/transported interface).

3 REGOLITH STRATIGRAPHY

3.1 REGOLITH EVOLUTION

The residual regolith at the Argo Au deposit and at the southern end of the Apollo mineralisation is incised by an east-west trending palaeochannel, which is part of the Lefroy Palaeodrainage (Figure 1). The regolith history of the Lefroy region has been described by previous workers (e.g., Carey and Dusci, 1999; Clarke 1994a,b,c; Clarke et al., 1994; Woolrich, 1994; Zheng et al., 1998) and can be summarized as follows:

1. The Archaean bedrock was probably weathered between the Late Permian and Middle Jurassic. The depth of weathering was variable, generally being shallow over mafic and granitic rocks, deeper over ultramafic rocks and deepest over sedimentary rocks (Clarke, 1994b).
2. From the Jurassic to Early Eocene, the Lefroy Palaeodrainage was incised into the weathered Archaean bedrock. The saprolite was commonly completely stripped over the mafics and in the deeper parts of the drainage system (Clark, 1994b).
3. In-fill of the palaeodrainage began during the Early Eocene with the fluvial deposition of gravels, sand and silts of the lower Pidinga Formation (Woolrich, 1994). A subsequent decrease in the palaeosystem’s energy led to the deposition of carbonaceous clays and lignitic sediments. The lignites are interpreted as overbank deposits. The Tortachilla transgression followed in the Middle Eocene and flooded the palaeodrainage to the modern day elevation of approximately 280 m and saw further deposition of the Pidinga Formation and Hampton Sandstone (Clarke et al., 1994).
4. In the Late Eocene, the Tuketja transgression (referred to as Aldinga transgression in some earlier literature), which was the more extensive of the two transgressions, reached the modern day elevation of 300 m (Clarke et al., 1994). During the Tuketja transgression, further Pidinga Formation and Hampton Sandstone sediments were deposited along with the Princess Royal Spongolite. The Princess Royal Spongolite was deposited in a low energy estuarine environment during the transgressional maximum (Clarke, 1994a).
5. Decreased rainfall and increasing seasonality from the end of the Eocene led to the disorganization of the palaeodrainage (Clarke, 1994b) and significant flow in the palaeorivers probably ceased before the mid-Miocene (Zheng et al., 1998). The Revenge Formation was deposited in a permanent to semi-permanent lacustrine environment (Zheng et al., 1998). Some deep weathering continued, most notably affecting the palaeodrainage fill, but also occurring under reducing conditions at the fill and bedrock interface (Clarke, 1994b).
6. With increased aridity, there was a lithological change from the siliciclastic Revenge Formation to the evaporitic Roysalt Formation. Zheng et al., (1998) give an age of Middle Pleistocene to Holocene based on palaeomagnetism but Clarke (1994c) gives an earlier age based on palynological evidence which suggests the change took place in the Early Pliocene. This arid phase has resulted in the modern day low topographic contrast and salt lake regime.

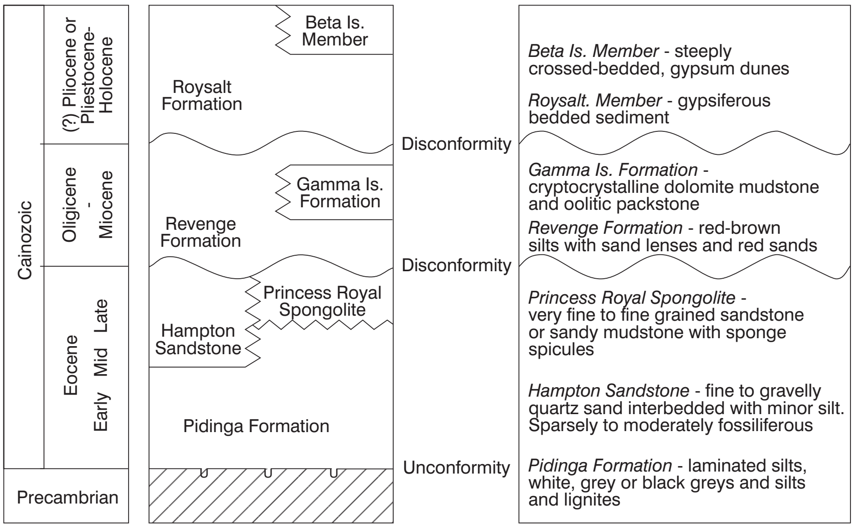

Figure 6: Nomenclature and description of the regional Lefroy stratigraphy (after Carey and Dusci, 1999)

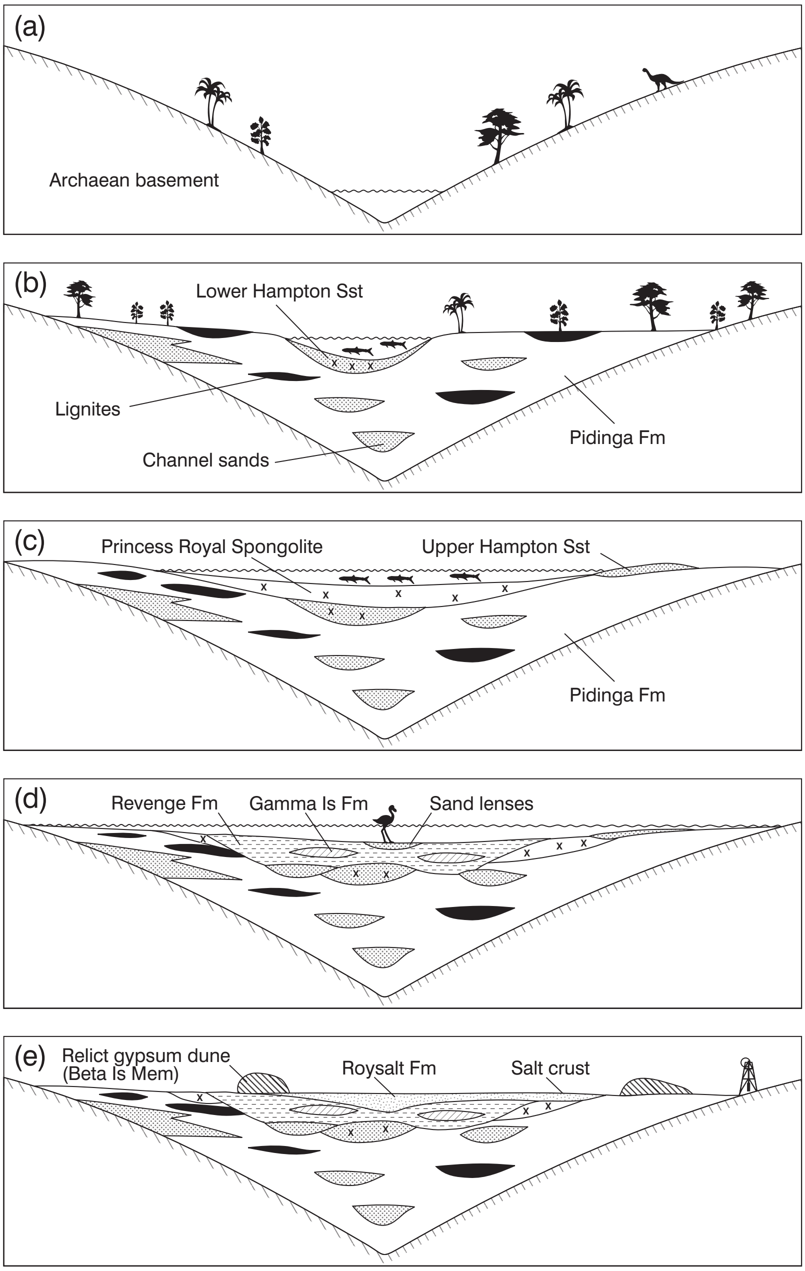

(a) Incision of the palaeodrainage system (pre-Jurassic).

(b) Middle Eocene Tortachilla transgression.

(c) Late Eocene Tuketja transgression.

(d) Semi-permanent lake stage (Miocene).

(e) Pliocene-Quaternary playa lake, depositing Roysalt Formation.

Figure 7: Schematic stratigraphic evolution of the Lefroy palaeodrainage (after Clarke, 1994a)

3.2 REGOLITH GEOLOGY

The regolith of the Argo-Apollo region consists of weathered Archaean rocks blanketed by sediments. The Archaean derived regolith of the Lake Lefroy region is described by Carey and Dusci (1999) as consisting of:

1. A lower saprock zone characterized by joint oxidation and minor oxidation of mafic minerals and sulphides.
2. An overlying saprolite with textures preserved, though the primary minerals have been dominantly replaced by weathered products.
3. An upper clay zone characterized by the complete replacement of original textures and mineralogy.
4. Rare lateritic duricrust.

All these units, except for lateritic duricrust, are present at Argo. However, the residual clay zone is sometimes ferruginized at the top.

The sedimentary units present in the Argo palaeochannel are described in Butt et al. (1997) as consisting of:

5. A basal unit of fluvial gravels, sand and lignitic silts, up to 16 m thick.
6. Overlying grey clays, about 30 m thick, containing carbonaceous woody fragments and lignite.
7. Spongolite, about 15 m thick, consisting of pale silts with about 50-60% siliceous sponge spicules.
8. An uppermost channel unit consisting of mottled lacustrine clays about 10 m thick.

Blanketing the entire Argo-Apollo region are another three transported units, described in Butt et al. (1997) as:

9. A unit of hard mottled red and grey clays. These contain zones of indurated ferruginous and siliceous material, forming a pan of variable thickness, generally between 2-7 m depth.
10. An overlying calcareous clay-rich red soil, 20 cm to 2 m thick with locally abundant calcrete nodules. Carbonates coat the clay peds and lithorelics in the soil and form cutans on the nodules. A dark manganiferous horizon occurs at 1.5 m depth.
11. An uppermost unit consisting of sandy aeolian topsoil, about 20 cm thick but reaching 2 m in places.

Primary and secondary mineralization is confined to the bedrock, saprock, saprolite and residual clay units as well as the unconformity with the transported material.

3.3 COMPARISON OF REGOLITH STRATIGRAPHIES

The thirteen layers used for modelling the regolith stratigraphy are described in Section 2.2 and Table 1. These regolith layers and their correlation with the regional and local stratigraphy described above are diagrammatically represented in Figure 8.

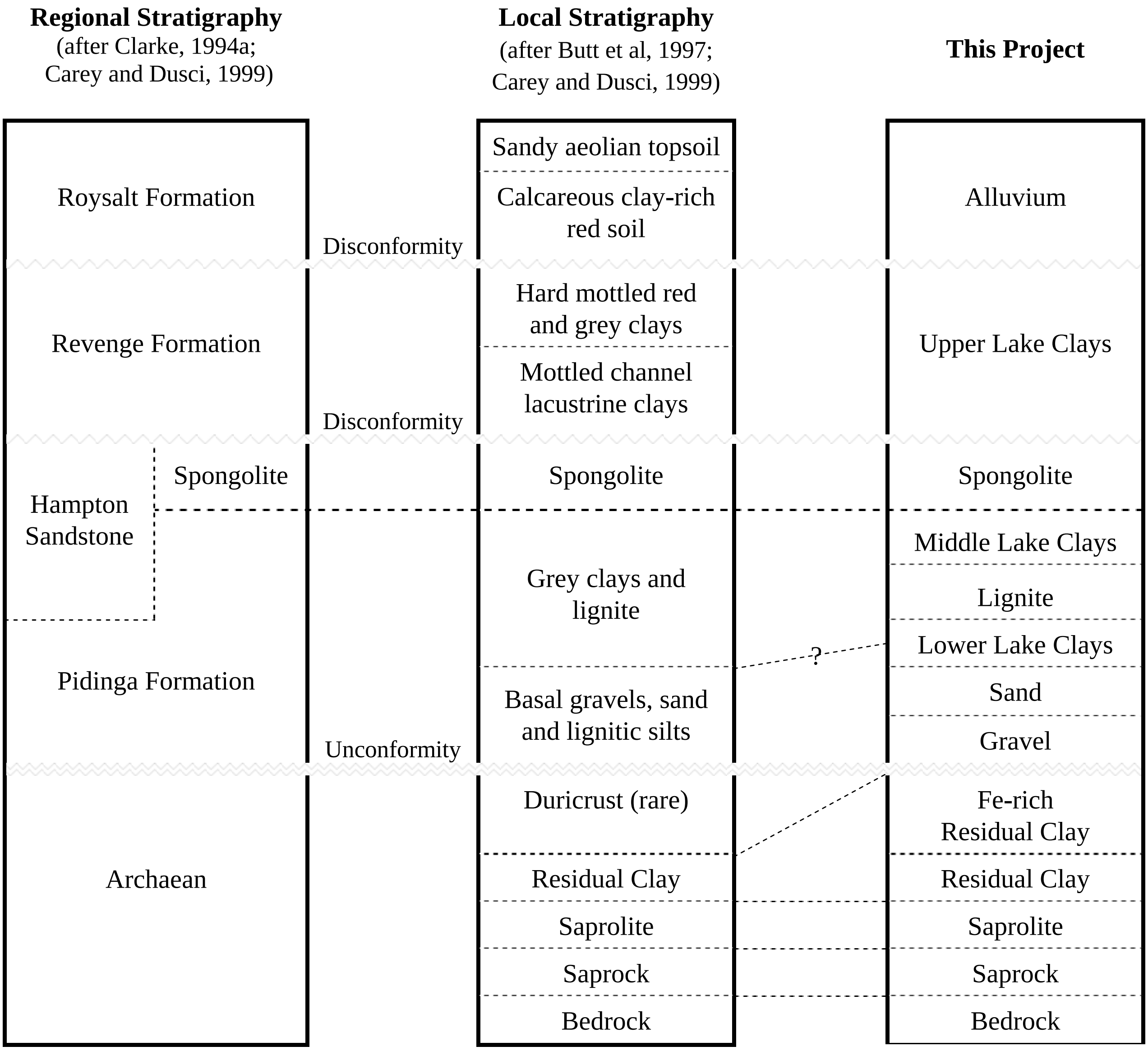

Figure 8: Comparison of the regolith layers used in this project in relation to the regolith stratigraphy of the Argo-Apollo deposits and the stratigraphy of the greater Lefroy region.

3.4 RESULTS

Results of the regolith modelling show two narrow chasms in the weathering front along the strike of the two NNE trending mylonitic shear zones associated with the mineralization (Section 1.4), with highs on either side of the shears. Bedrock forms a low under the palaeochannel and to the east (Figure 9).

Weathering has produced saprock, saprolite and residual clay of varying thickness over the region (Figure 10). Generally, the residual clay unit appears to be the thickest unit, but it, the saprolite and, sometimes, the saprock are thinner beneath the palaeochannel. Additionally, some upper parts of the residual clay unit in upland areas have been ferruginized (but are not duricrust) (Figure 11).

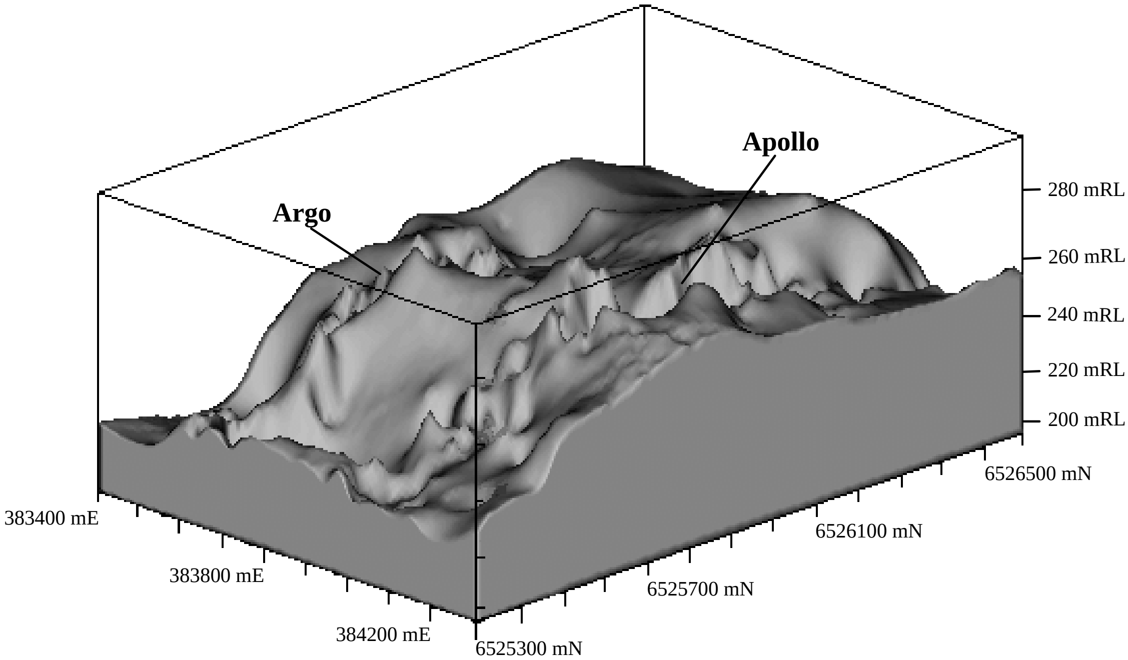

Figure 9: Modelled base of weathering for the Argo and Apollo gold deposits. Mineralization is associated with two narrow NNE trending mylonitic shear zones that form narrow lows at the weathering front.

Within the sediments, the basal gravel and sand units are mostly confined to the palaeochannel, though patches fill depressions in some upland areas (Figure 10). Lake clays cover most of the region and are, predictably, thickest in the palaeochannel. The lignite- and spongolite-dominated layers are mostly confined to the palaeochannel and, like the sand and gravel, also fill some upland depressions (Figure 10). The interfaces between the lake clays, lignite and spongolite are irregular. There is almost no indication of the palaeochannel as a topographic low at the surface or the top of the upper lake clays. The alluvium is the most uniformly thick regolith layer (Figure 10).

3.5 DISCUSSION

Regolith modelling indicates a highly irregular boundary between the saprolite and saprock (Figure 10). As noted in Section 2.2, the logging of this boundary was not as consistent as for other interfaces, which is probably a reflection of its typically transitional nature. Thus, in most instances, these layers would be best treated as a single unit when assessing the modelling results.

Of the residual regolith units, the residual clay appears to be the thickest, at least in the upland areas (Figure 10). In the palaeochannel it thins considerably and modelling suggests that it, along with the underlying saprolite in some places, has been eroded. This correlates with Clarke (1994b) who states that "… the weathered regolith largely predates the incision of the palaeodrainage." He also notes that the deepest parts of both the Lefroy and nearby Cowan palaeodrainage have cut through the regolith to fresh rock.

The ferruginous residual clay is mostly confined to the upland areas and hill flanks of the pre-Eocene landscape (Figure 11). Given that some of the residual clay and saprolite in the palaeochannel appears to have been eroded, it is possible that the ferruginous residual clay layer was once more extensive but has also been eroded. Scattered patches of the ferruginous clay in the palaeochannel suggest that this might have been the case. It is also possible that it was never present in the palaeochannel to any great extent and that the ferruginization of the residual clay in the higher landscape reflects past suitable redox conditions and/or water tables in these positions. There is no evidence to suggest that lateritic residuum (duricrust) was ever developed on the residual weathering profile; certainly no lateritic sediments have been found in the basal sediments of the palaeochannel (M. Carey, WMC, personal communication, 1999). It is also probable that the ferruginization of the residual clay occurred prior to burial by lignitic sediments, as these create a reducing rather than an oxidizing environment.

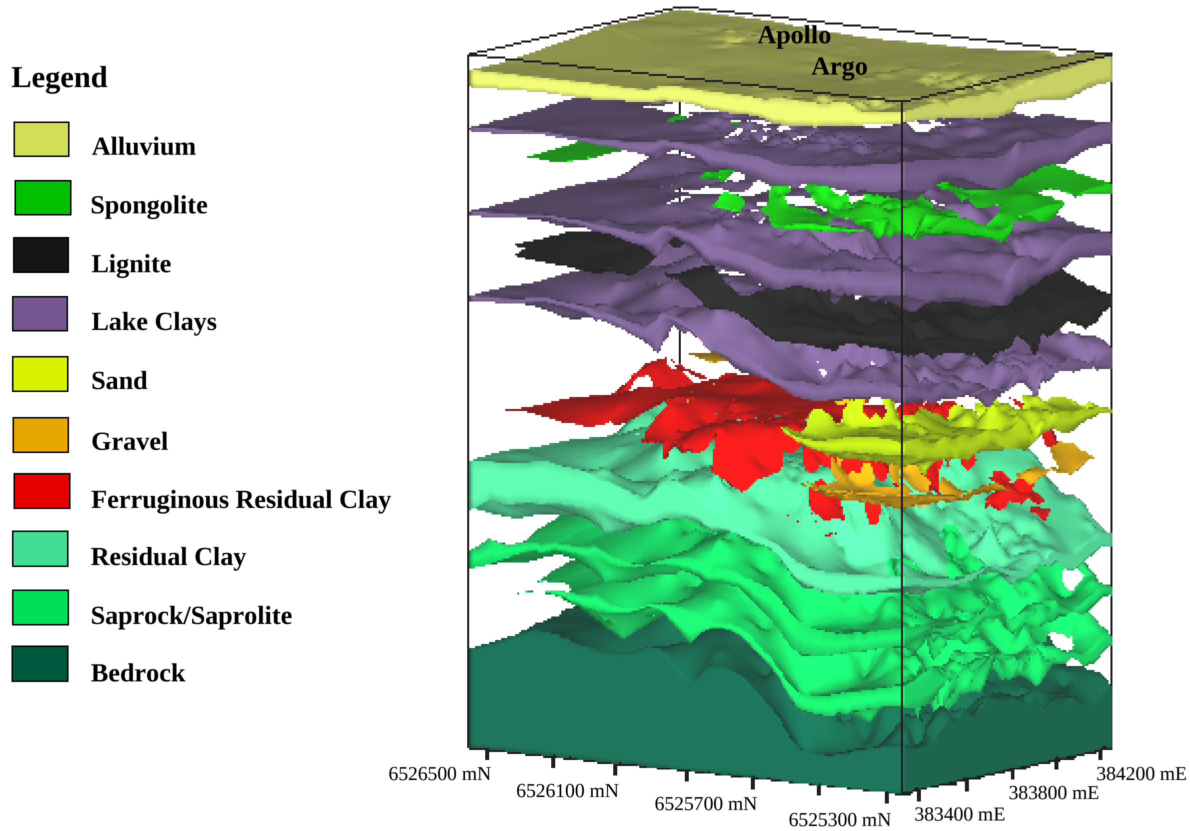

Figure 10: Regolith stratigraphy of the area around the Argo and Apollo deposits, looking north-east

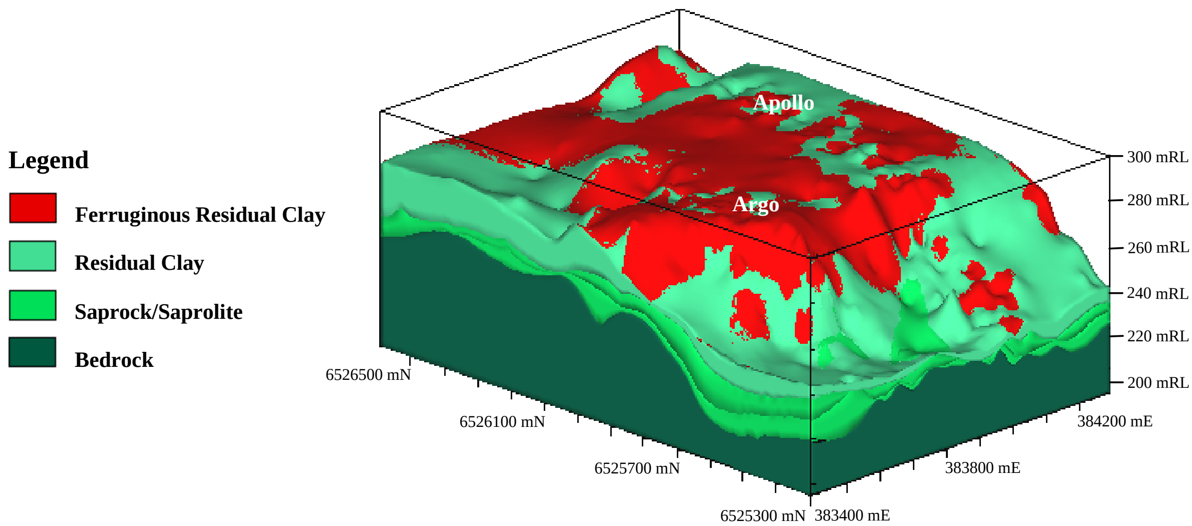

Figure 11: Ferruginous residual clay draping over the uplands and down the palaeoslopes. Note also that the residual clay layer appears to be eroded in the palaeochannel. View looking north-east.

The boundary between the lake clays and the lignite- and spongolite-dominated layers is irregular. This might be a result of the method used to define the boundaries (section 2.1), but the boundary between the middle lake clays and the spongolite may, at least in places, be real. Clarke (1994a) discusses the erosion of the upper Pidinga Formation prior to deposition of the Princess Royal Spongolite during the second Eocene marine transgression. Similarly, the regolith stratigraphy of Clarke (1994a), Butt et al (1997) and Carey and Dusci (1999) (Figure 8) also indicates that the lake clays overlying the spongolite are part of the Revenge Formation. These two layers, the spongolite and upper lake clays, can, therefore, for the most part, be regarded as distinct sedimentary units when assessing the stratigraphic model. Overall, the occurrence and geometry of each regolith layer defined in the model correlates well with the regolith stratigraphies described by previous workers in the Lefroy region.

4 GOLD DISTRIBUTION

4.1 ARGO-APOLLO REGION

Bedrock mineralization can clearly be seen running along two narrow north-south trending zones (Figure 12), identified as the mylonitic shear zones described in Section 1.4. Gold content is variable but strongest at the Argo deposit. Regional cross sections show background Au concentration for all regolith layers is patchy but generally less than 100 ppb. In the vicinity of mineralization, Au concentration in the residual profile is generally between 100 ppb and 1 ppm. Some higher Au concentrations (>10 ppm) occur in bedrock and there appears to be supergene enrichment in the saprock, saprolite and residual clay (also >10 ppm) (Figure 13). The diagrams of Au distribution at the interface of each regolith layer show that Au contents are more extensive in the saprock and saprolite (Figure 14a). Gold concentration is low at the top of the residual clay, (mostly < 200 ppb; Figure 14b) but, at the southern end of the deposits, mineralization is still exposed in the palaeochannel, especially at Argo.

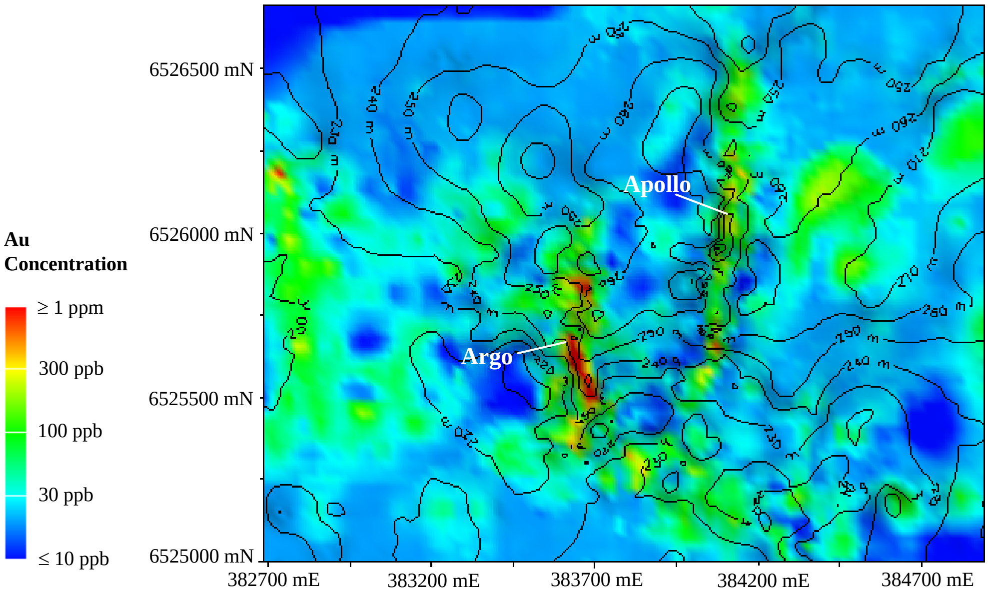

Figure 12: Gold distribution at the weathering front across the Argo-Apollo region, with topographic contours of the weathering front shown in black.

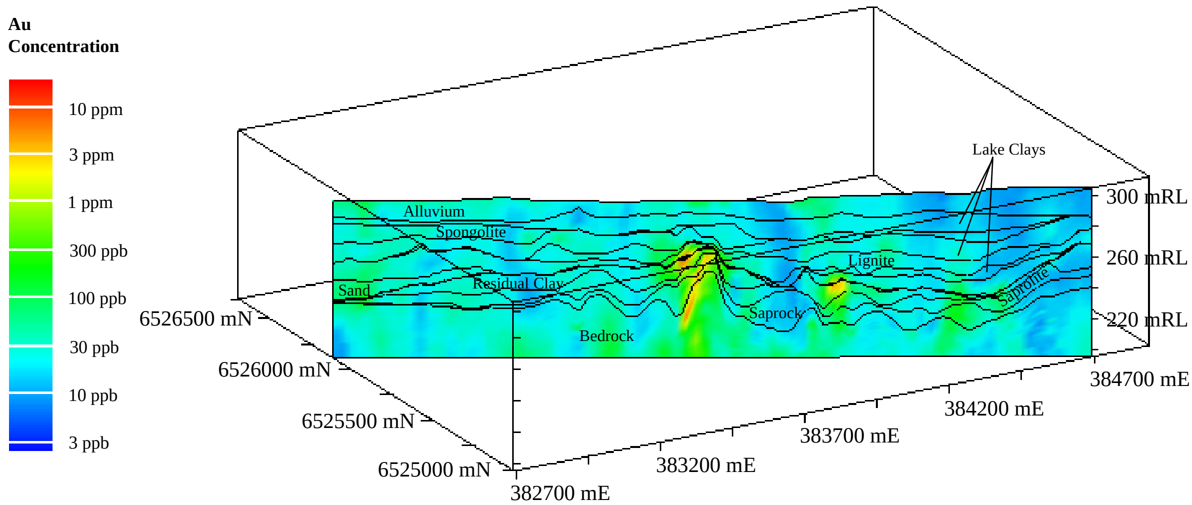

Figure 13: Gold distribution in regional cross-section along strike with palaeochannel.

The lake sediments infilling the palaeochannel, especially the gravel and sand, contain less than 30 ppb, except where they overlie, or are close to, mineralization in the residual profile (Figure 13). Thus, the gravel and sand, and, to a lesser degree, the lower lake clay and lignite layers have high Au content in the vicinity of mineralization. The surface appears to be somewhat more enriched than the upper lake sediments (Figure 14c). However, a large part of this surface enrichment is probably spurious, due to cross-hole contamination. Four auger soil traverses across the Argo surface (Lintern and Gray, 1995) gave a maximum 24 ppb Au, in contrast with concentration commonly greater than 100 ppb Au found in the exploration drilling.

4.2 APOLLO DEPOSIT

Gold concentrations greater than 1 ppm in the bedrock along the Apollo mineralized zone are patchy but become more strongly developed in the saprock (Figure 14a). Indications of mineralization along the Apollo mineralized zone are still present at the gravel/sand and sand/lower lake clay interfaces. Concentrations are less than 200 ppb at the overlying lower lake clay/lignite interface, except in the north where small amounts of lake clays have Au content above 500 ppb where this interface is close to the unconformity. All signs of mineralization are obliterated by the deposition of lignite. Gold abundances at the middle lake clay/spongolite, spongolite/upper lake clay and upper lake clay/alluvium interfaces remain comparatively low (< 200 ppb). Patchy enrichments to > 500 ppb Au in the alluvium that coincide with the Apollo mineralized zone (Figure 14c) are probably due to cross-hole contamination (Section 4.1).

4.3 ARGO DEPOSIT

4.3.1 Interface models

The diagrams of Au distribution at the interface of each regolith layer (Figure 14) show that the Argo and Apollo mineralized zones are similar, although mineralization at Argo is more extensive. Modelling shows enrichment at the saprock/saprolite (Figure 14a) and saprolite/residual clay interfaces with Au concentrations ≥ 1 ppm. Conversely, the residual clay/ferruginous residual clay interface and the unconformity are depleted compared to the saprolite and saprock (Figure 14b). Gold concentrations in the “upland” areas are mostly less than 30 ppb, but in the palaeochannel, Au concentrations ≥ 1 ppm outcrop in the channel slope and floor.

The gravel/sand interface, mainly restricted to the palaeochannel, also has Au concentrations greater than or equal to 1 ppm in areas corresponding to the mineralization in the underlying residual regolith. The sand/lower lake clay interface mostly has Au concentrations less than 200 ppb but mineralization in the residual material is still “exposed” in the channel side. Gold contents in the lower lake clays are similarly low (mostly < 30 ppb) but concentrations ≥ 1 ppm coincide with the underlying mineralization in the channel side, but to a lesser extent than the underlying sediments. The lignite/middle lake clay, middle lake clay/spongolite, spongolite/upper lake clay and upper lake clay/alluvium interfaces have less than 200 ppb Au. The alluvium at Argo, like Apollo, has several patches of Au concentration greater than 500 ppb coinciding with mineralization (Figure 14c) but these are probably due to cross-hole contamination (Section 4.1).

4.3.2 Three-dimensional models

The bedrock mineralization at Argo can be clearly seen in the 1 ppm Au cut-off model (Figure 15a). Mineralization can be seen running in a main shoot up the palaeoslope and a second smaller shoot can be seen branching off and terminating approximately 10 m under the palaeochannel floor, though scattered pods of high-grade bedrock continue to trend upwards to the weathering front. Other pods of high-grade mineralization in the bedrock can also be seen trending northwards along the mineralized zone.

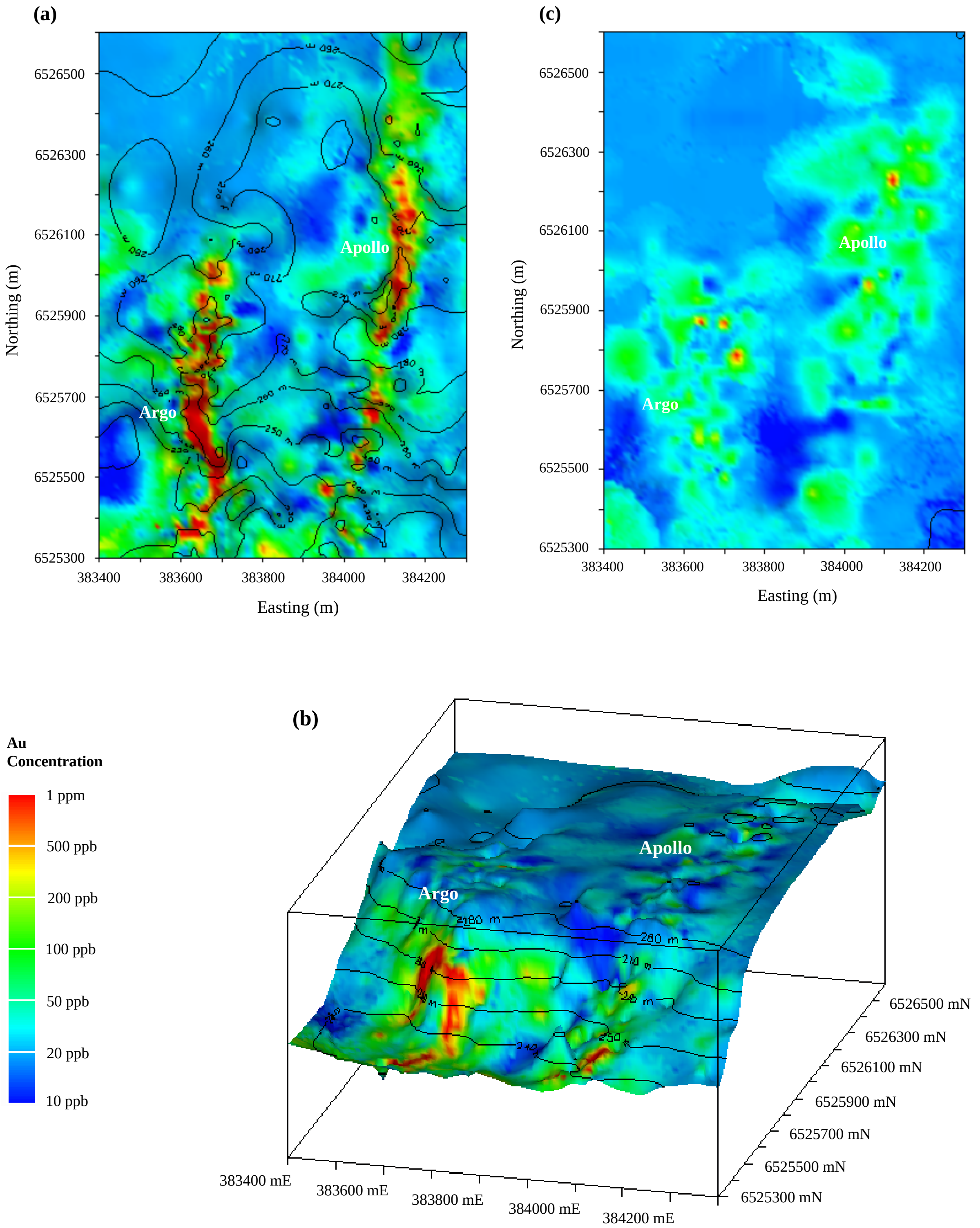

Figure 14: (a) Plan view of Au distribution at the saprock/saprolite interface. (b) View of the unconformity showing Au distribution in relation to the palaeochannel. "Upland" areas are depleted in gold but mineralisation in still "exposed" in the palaeochannel. (c) Plan view of Au distribution at the ground surface. The areas of high gold concentration correlate with the mineralized zones shown in (a), but are thought to be due to cross-hole contamination.

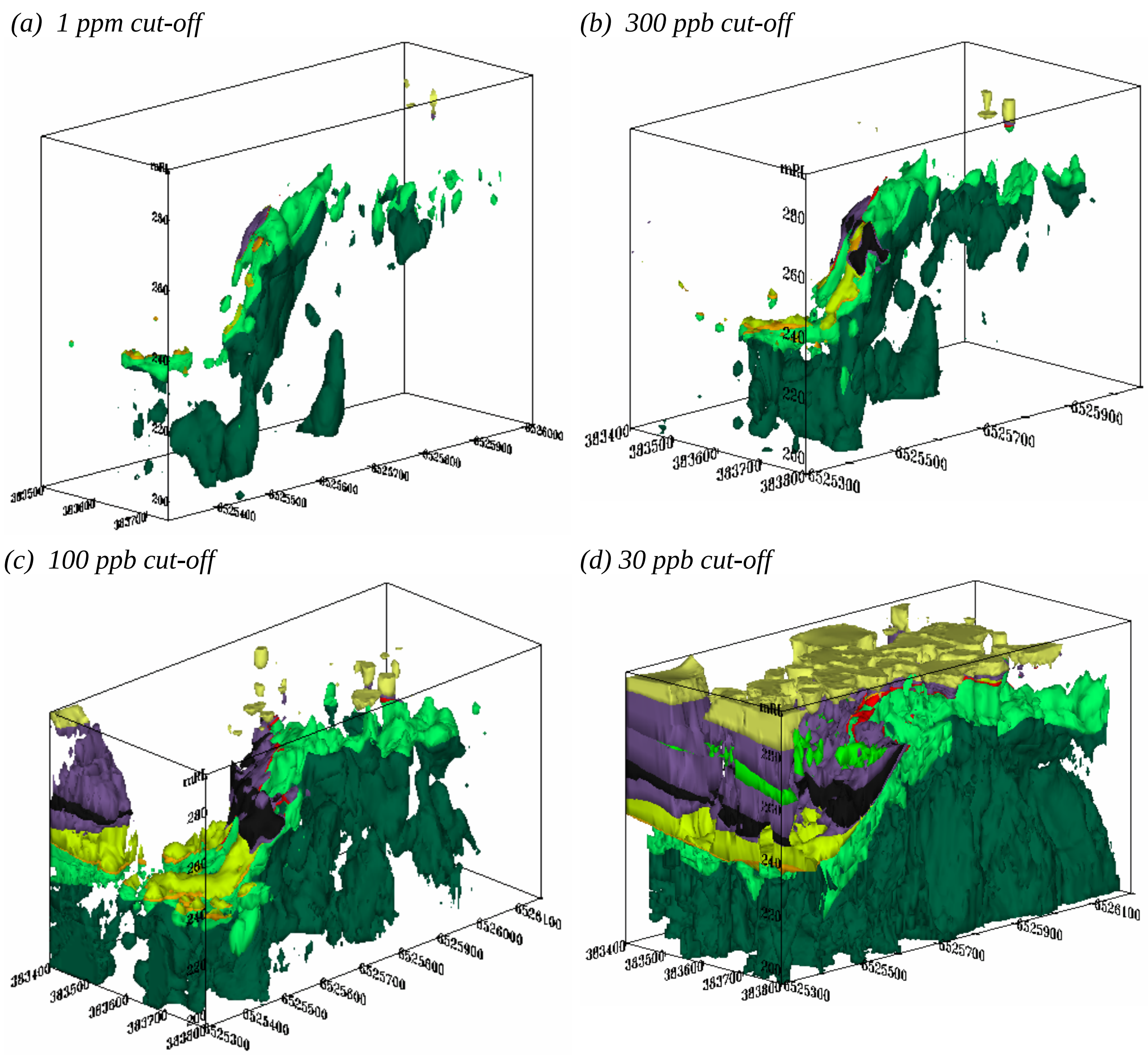

Figure 15: Gold distribution at Argo, using (a) 1 ppm, (b) 300 ppb, (c) 100 ppb and (d) 30 ppb cut-offs. Where Au concentration is greater or equal to the cut-off, the area is coloured according to the regolith horizon (Table 3, Figure 10).

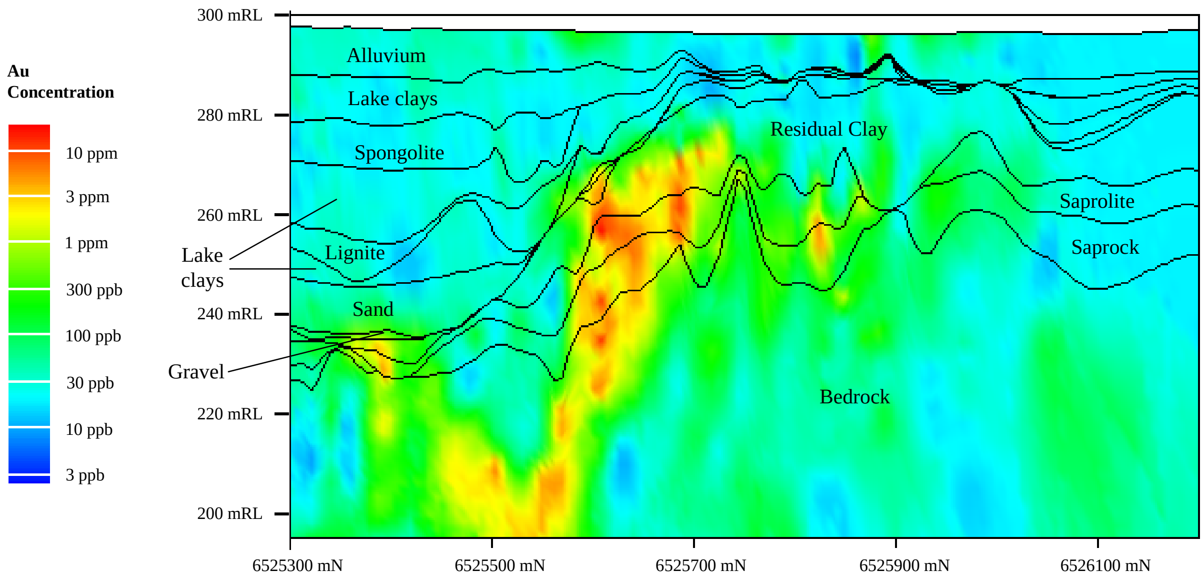

Figure 16: Gold distribution for the N-S cross section at 383630 mE through the Argo deposit.

The residual regolith mostly has Au concentrations of 1 ppm or greater only where it is developed over bedrock of similar grade (Figure 15a). The exceptions are the residual regolith developed in the palaeochannel floor and some patches at the northern end of the mineralized zone. The bedrock beneath both areas has Au values mainly between 300 ppb and 1 ppm with higher values occurring in some small scattered pods (Figure 15b). The residual regolith developed over the palaeochannel floor appears to be mainly supergene enrichment and it, the overlying gravel and some sand patches have Au values of 1 ppm or greater along the strike of the mineralized zone. Similarly, the patches of high-grade Au in the northern residual regolith indicate some degree of supergene enrichment.

Gravel, sand and lower lake clays abutting the mineralized palaeoslope also contain ≥ 1 ppm Au (Figure 15a). Much of the gravel and the lower portion of the sand unit have Au concentrations to 1 ppm and it appears that Au has dispersed along the mineralized palaeoslope to the channel floor in these lower sedimentary units. Approximately half of the sand unit has Au concentrations between 100 and 300 ppb. Lignite, where it abuts the mineralized palaeoslope, also contains 300 ppb to 1 ppm Au and most of the lignite, and some of the lower and middle lake clays, have 100 and 300 ppb Au adjacent to the mineralized palaeoslope (Figure 15c). The spongolite and most of the upper lake clay has less than 100 ppb Au. A few patches of alluvium have Au concentrations greater or equal to 1 ppm co-incident with the mineralized zone, but the vast bulk has Au values less than 100 ppb (Figure 15c). The three-dimensional models of Au distribution show that most of the regolith at Argo has at least 30 ppb Au content (Figure 15d).

4.3.3 Cross-sections

The cross-sections of Au distribution in the regolith suggest a depletion zone at Argo (Figure 16). Gold (≥ 10 ppm) is present in the saprock and saprolite, but only in the lower part of the residual clay unit. This possible depletion can also be seen in the regional cross-sections of Au distribution (Figure 13) as a subhorizontal zone at approximately 270-275 mRL.

4.4 DISCUSSION

4.4.1 The residual profile

Supergene enrichment in the residual regolith appears to be mostly strongly developed in the saprock, saprolite and lower portion of the residual clay, with Au ≥ 1 ppm generally only developed over bedrock of similar grade. The exceptions are in the palaeochannel floor and some patches at the northern end of the Argo mineralized zone, where bedrock concentrations are generally lower. This enrichment is possibly due to hydromorphic activity in the palaeochannel and beneath sedimentary cover in northern upland depressions. There is also some evidence to show that much of the gold in the palaeochannel is detrital. Gold grain analyses by Woolrich (1994) suggest that primary gold grains were modified before being eroded and deposited in the palaeochannel, as much as 400 m from source.

The cross-sections of Au distribution in the regolith profile indicate a sub-horizontal depletion zone at Argo (Figure 16) and across the general region (Figure 13), at approximately 270-275 mRL in the upper residual clay. Data from Lintern et al (1997, Appendix 1.4 and 1.5) suggest depletion of Ca and Mg and possibly As, Ce, La and Mn as well as Au at a similar depth (267-276 mRL).

4.4.2 Palaeochannel sediments

Lintern and Gray (1995) suggested that lignite might be scavenging Au at the Argo deposit. In their study, five lignitic samples were taken from two drill holes, one adjacent to the main mineralization, one away from the mineralization. Other materials were also taken from these two holes (Table 4) and results showed that the lignitic samples tended to have the higher Au concentrations (Table 4; Figure 17). However, in recognition of the limited data, no firm conclusions were drawn and further investigation was recommended.

Table 4: Sample locations, descriptions and Au concentrations in sediments (after Lintern and Gray, 1995).

Sample	Sample No.	Hole ID	Easting (m)	Northing (m)	Depth (m)	Material	Au (ppb)
a	09-1585	TD 3489	383420	6525800	9-10	Mottles	7
b	09-1666/67	TD 3798	383520	6525880	22-24	Pisoliths	<5
c	09-1591	TD 3489	383420	6525800	26.5	Lignitic	25
d	09-1590	TD 3489	383420	6525800	25.5	Buff/cream clay and grey lignitic material	85
e	09-1486	TD 3676	383580	6525840	3-4	Mottles	<5
f	09-1623/24	TD 3827	383525	6525620	5-7	Mottles	5
g	09-1625/26	TD 3827	383525	6525620	7-9	Mottles	<5
h	09-1629/30	TD 3827	383525	6525620	11-13	Mottles	<5
i	09-1655	TD 3827	383525	6525620	37.5	Lignitic	229
j	09-1658	TD 3827	383525	6525620	40.5	Lignitic	28
k	09-1657	TD 3827	383525	6525620	39.5	Pale grey clay with some lignitic material	67
l	09-1661/62	TD 3827	383525	6525620	50-52	Pisoliths	100
m	09-2298	TD 3718	383594	6525620	5.5	Ferruginous silicified clay	<5
n	09-2300	TD 3718	383594	6525620	8.5	Fe-segregations	<5
o	09-2303	TD 3718	383594	6525620	21.5	Shaley clay	<5

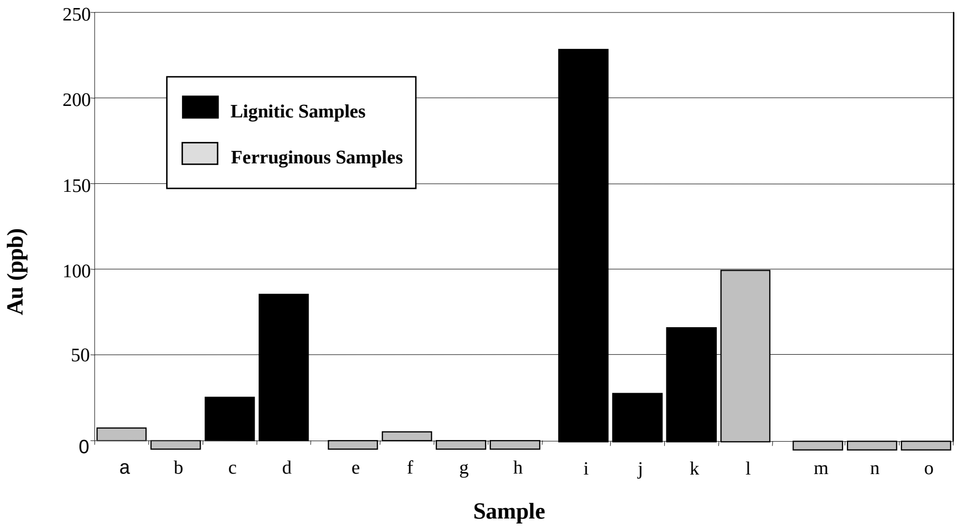

Samples a-d: furthest from mineralization
Samples e-h: super-adjacent to mineralization (from the upper profile)
Samples i-l: adjacent to mineralization
Samples m-o: above mineralization

Figure 17: Gold abundances for ferruginous and lignitic samples hand-picked from transported overburden at Argo. Negative data is below detection. From Lintern and Gray (1995).

Lignite samples (i), (j) and (k) were collected adjacent to the mineralization and close to the unconformity (Table 4; Figure 17). Sample (l) from the same drill hole has a comparable amount of Au though it is closer to the unconformity (Figure 17). The modelling results from this study show that all sediments in this area have high Au concentrations and lignite does not stand out as being more anomalous (*e.g.*, Figure 16). Lignitic samples (c) and (d) were taken from a drill hole away from the main mineralization but close to the unconformity (Table 4; Figure 17). The modelling results show that there is also a higher than background abundance of Au in the residual regolith and lower channel sediments at this location (Figure 16). Sample (a), to which the lignitic samples are compared, is from higher in the profile (Table 4; Figure 17). Modelling shows that Au contents decrease up profile from the unconformity (Figure 16); thus, material from higher in the profile would be expected to have less Au than materials closer to the unconformity, in this case, lignite. Sample (b), to which the lignite samples were also compared (Table 4; Figure 17), is from a similar depth but from a drill hole in an area of background Au concentration (Figure 15).

Iron mottles and Fe-clays [samples (e-h), (m) and (n)] from the top 13 m of the profile have low Au concentration (≤ 5 ppb) (Table 4; Figure 17), which is in agreement with the findings of this study. Sample (o), however, is from deeper in the profile, over mineralization, but it too has low Au concentration (≤ 5 ppb) and appears to be from the depletion zone.

This study indicates that Au concentrations in lignite are very much dependent on position in relation to the mineralization and the unconformity, and that lignite is not necessarily more anomalous in Au than other materials.

5 GOLD CONCENTRATION CALCULATIONS

5.1 ARGO DEPOSIT

Calculations of the volume of each regolith layer at the Argo deposit (Figure 18) show that saprock (13%) and saprolite (12%) have similar volume, but that residual clay is the largest regolith unit (20%). Ferruginous residual clay and gravel have the least volume (1.2% and 0.4%, respectively). There is slightly more sand (4.9%), lignite (4.0%) and spongolite (3.4%) with the remaining lake clay units accounting for 27% of the regolith. The alluvium has a volume of 15%.

Calculations of mean Au concentration for each layer (Figure 19) show that saprock (413 ppb) and saprolite (542 ppb) are enriched compared to bedrock (261 ppb). Residual clay (300 ppb) is also slightly enriched compared to bedrock but not compared to saprolite and saprock. The ferruginous residual clay has significantly less Au (111 ppb). These lower values for the residual clay units are due to the much lower Au concentrations above approximately 276 mRL. For example, if the ferruginous residual clay is split into > 276 mRL and < 276 mRL fractions (the Argo case in Table 5), the fraction > 276 mRL, which comprises 80% of all of the ferruginous residual clay, has a mean Au concentration of only 37 ppb. In comparison, the fraction < 276 mRL has a much higher mean Au content of 412 ppb. Thus, if only the < 276 mRL fractions of the *in situ* regolith units are compared (Table 5), there is not a significant Au depletion for the residual clay units. In addition, the fact that depletion is observed for all *in situ* regolith units at the same elevation suggests that the effect cross-cuts regolith stratigraphy and presumably post-dates the major weathering.

The basal gravel unit has the highest mean Au (1535 ppb), approximately three times that of the saprolite, suggesting major Au concentration at the base of the palaeochannel. The Au content of the sand is also high (650 ppb) but declines in the lower lake clays (186 ppb), lignite (148 ppb) and middle lake clays (101 ppb). Spongolite has the least Au (31 ppb) but Au concentration is slightly higher in the upper lake clays and alluvium (79 ppb and 54 ppb, respectively).

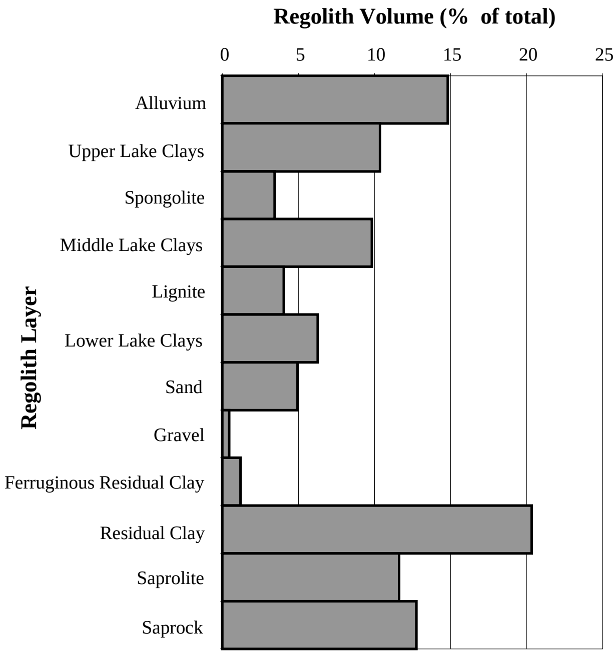

Figure 18: Comparative volume of each regolith layer from the Argo deposit, as a percentage of the total regolith volume.

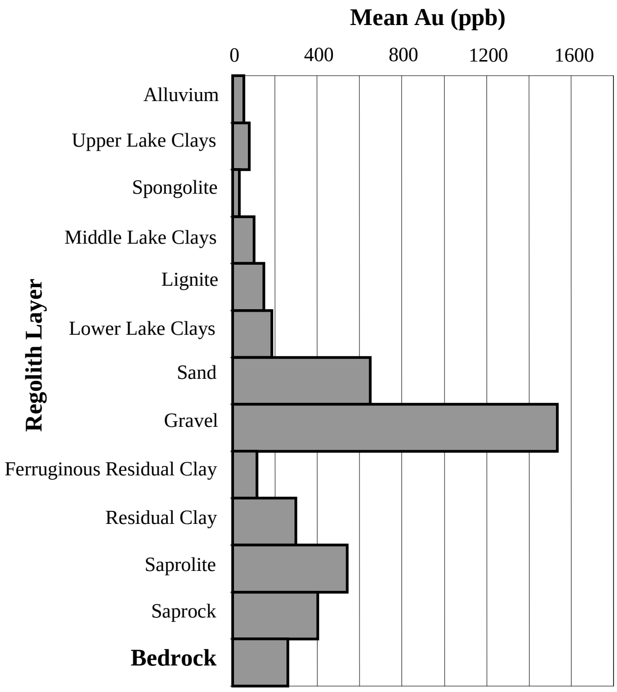

Figure 19: Mean Au concentration for each regolith layer and bedrock from the Argo deposit.

Table 5: Gold concentrations and mass ratios for saprock, saprolite, residual clay and ferruginous residual clay, split into > 276 m and < 276 mRL component, for the Argo deposit, Argo channel and Apollo deposit.

			Argo	Channel	Apollo
Ferruginous Residual Clay	Mean Au (ppb)	All	111	1245	36
		>276 m	37	93	35
		<276 m	412	1255	57
	(>276 m)/(<276 m) ratio (%)	Au	9	7	62
		Mass	80	1	96
Residual Clay	Mean Au (ppb)	All	300	949	145
		>276 m	48	92	84
		<276 m	388	949	229
	(>276 m)/(<276 m) ratio (%)	Au	12	10	37
		Mass	26	0.0004	58
Saprolite	Mean Au (ppb)	All	542	706	342
		>276 m	52	-	84
		<276 m	546	706	392
	(>276 m)/(<276 m) ratio (%)	Au	10	-	22
		Mass	1	0	16
Saprock	Mean Au (ppb)	All	413	473	289
		>276 m	28	-	88
		<276 m	414	473	313
	(>276 m)/(<276 m) ratio (%)	Au	7	-	28
		Mass	0.04	0	11

5.2 ARGO CHANNEL

Calculations of the volume of each regolith layer in the Argo palaeochannel (Figure 20) show that saprock (11%) and saprolite (9%) have similar volume. There is less residual clay (6.3%) and almost no ferruginous residual clay (less than 0.1%). Of the sediments, the gravel layer has least volume (0.9%). There is significantly more sand (11%) which is overlain by lower lake clays and lignite making up 7% and 6% of the regolith respectively. The middle lake clays (14%) and upper lake clays (15%) are significant proportions of the total volume, with the spongolite between making up 7% of the regolith. Alluvium makes up 12% of the regolith volume.

Calculations of mean Au (Figure 21) show that, of the residual regolith units, saprock has the mean Au (473 ppb), but saprolite (706 ppb) has a similar amount to bedrock (736 ppb). The residual clay and the small amounts of ferruginous residual clay have significantly more Au (949 ppb and 1245 ppb, respectively). The comparatively higher concentrations for the residual clay units, relative to the results for the entire Argo site, is presumably due to the fact that this area is under the deep palaeochannel and nearly all of the residual clay is below 276 mRL (Table 5), and therefore not depleted. Of the transported units, the gravel layer has the highest mean Au (1636 ppb) which is also the highest concentration of all of the regolith units. The sand also has significant Au content (652 ppb) but this progressively decreases in the overlying lower lake clays (287 ppb), lignite

(168 ppb) and middle lake clays (133 ppb). Spongolite has the least Au (30 ppb), but Au content is higher in the upper lake clays (100 ppb) and alluvium (39 ppb).

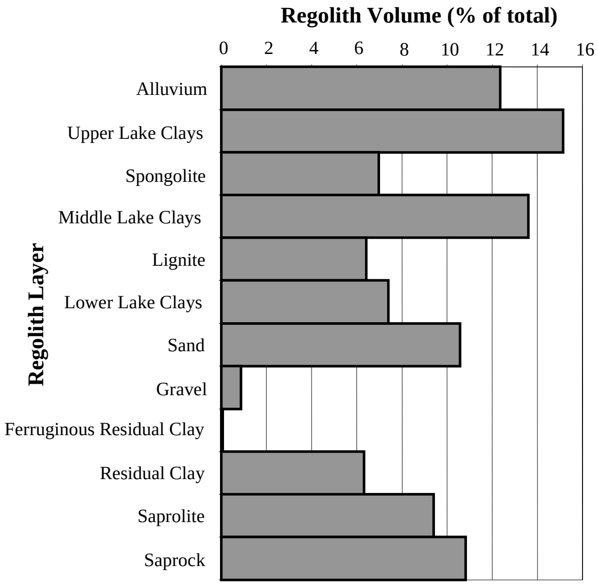

Figure 20: Comparative volume of each regolith layer from the Argo palaeochannel, as a percentage of the total regolith volume.

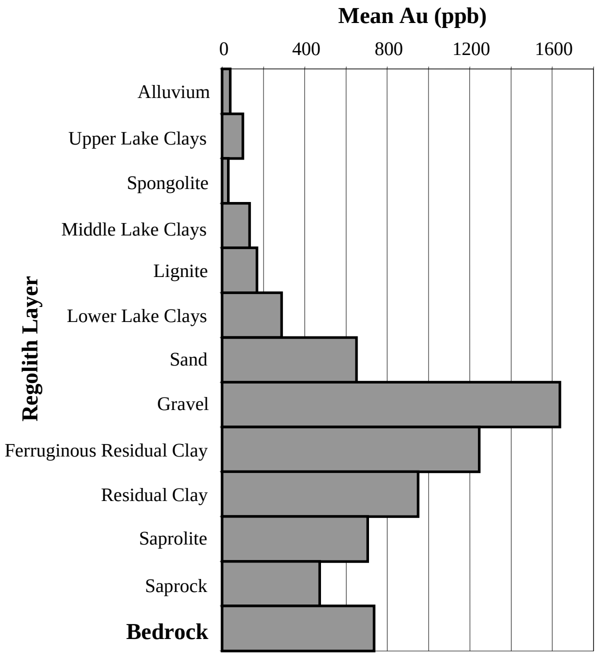

Figure 21: Mean Au for each regolith layer and bedrock from the Argo palaeochannel.

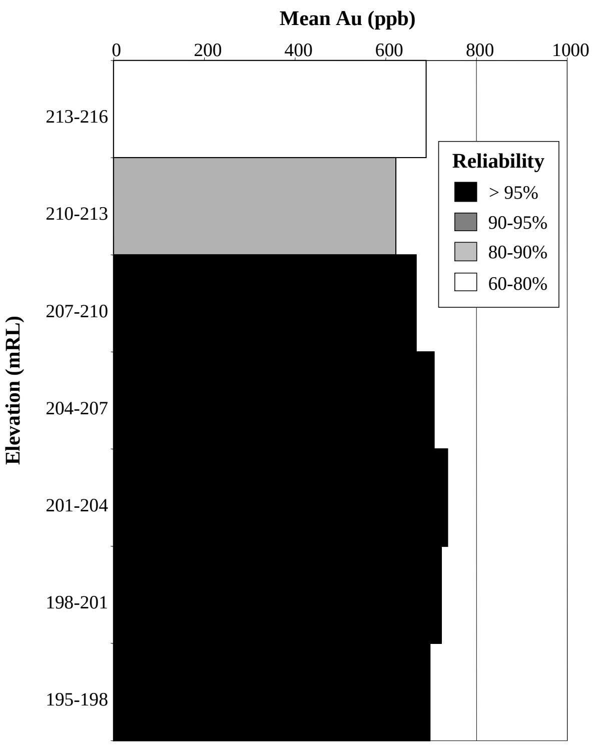

Figure 22: Mean Au vs elevation in bedrock at the Argo palaeochannel

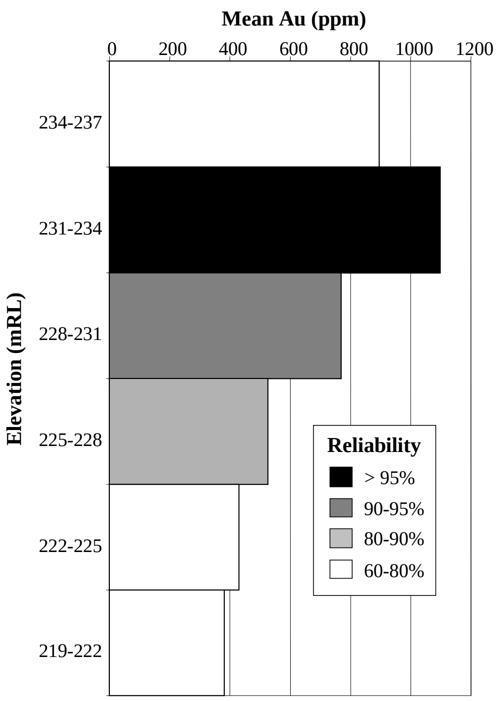

Figure 23: Mean Au vs elevation in the residual regolith at the Argo palaeochannel.

Further calculations of mean Au contents in the palaeochannel at the Argo deposit were based on 3 m thick horizontal slices of transported material, residual regolith and bedrock (Figures 22 to 25). The reliability of the results of each slice have been calculated using the method described in Section 2.4. Only the data for those slices considered 60% reliable or greater are shown.

Gold concentration is fairly homogenous in the bedrock (Figure 22) but may be increasing up-profile in the residual regolith (Figure 23). Data of 60% or greater reliability was, however, limited for both bedrock and residual regolith. In contrast, in the transported material mean Au content decreases up-profile from the unconformity (Figure 24).

Comparing mean Au concentrations in the bedrock, residual regolith and transported regolith against depth (Figure 25) shows Au in the bedrock increasing steeply in the upper residual profile at about 225-228 mRL and peaking at 231-234 mRL. It then decreases in the transported sediments, at first sharply to about 246-249 m and then more gradually from this point to the surface at about 294 m.

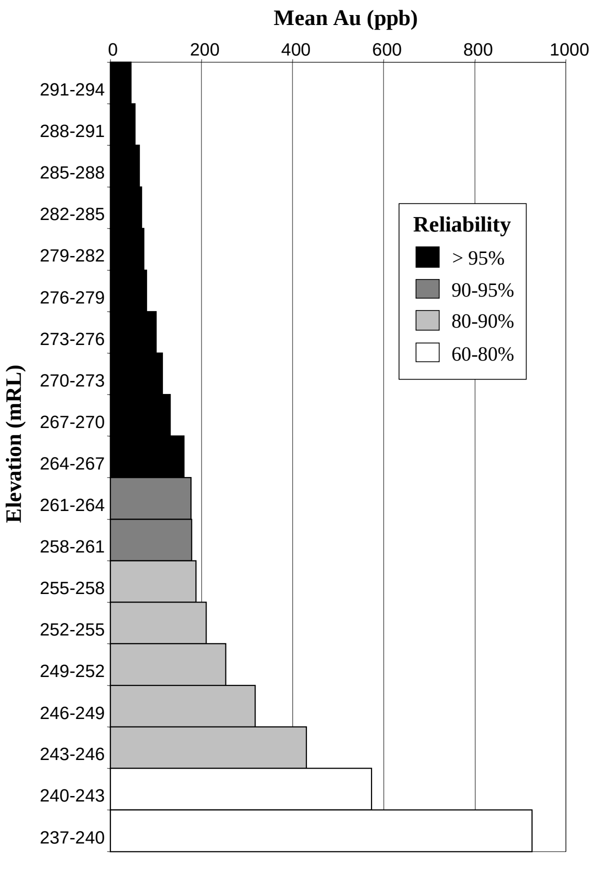

Figure 24: Mean Au vs elevation in the transported regolith at the Argo palaeochannel.

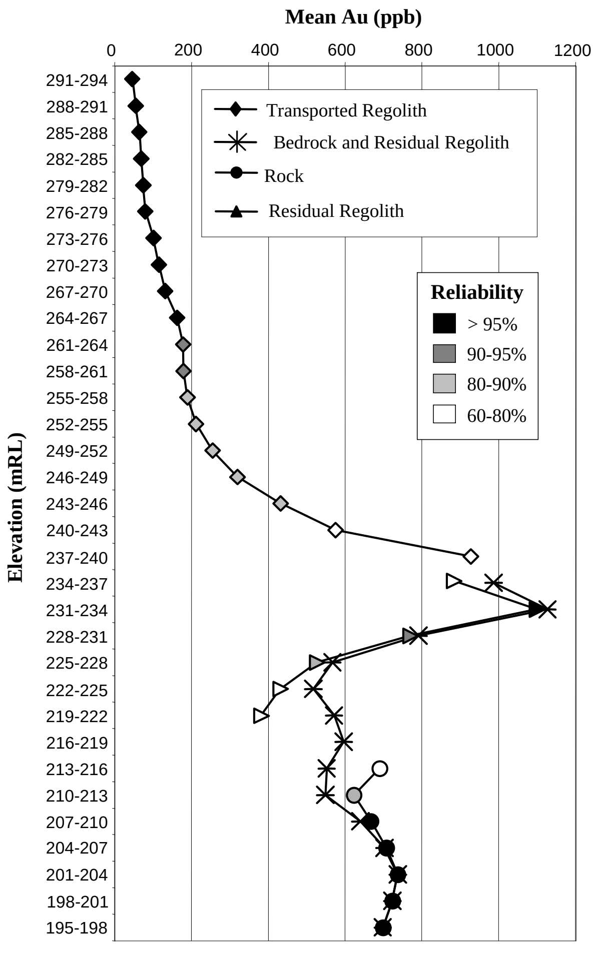

Figure 25: Mean Au vs elevation for all regolith at the Argo palaeochannel.

5.3 APOLLO DEPOSIT

At the Apollo deposit, there is significantly more saprock (27%) than saprolite (9%) (Figure 26). Residual clay (32%) is the dominant residual regolith unit, with a further 1.3% ferruginous residual clay. Of the transported units, gravel and sand are insignificant (both approximately 0.1%). The lake clay sediments have more volume (8% in total) over the Apollo deposit and small amounts of lignite and spongolite are present (both approximately 0.6%). Alluvium (22%) makes up a significant percentage of the regolith. Note that the northern Apollo area was deliberately chosen as an area with little or no palaeochannel sediments, so as to focus on calculating Au concentrations and statistics for the residual profile.

Calculations of mean Au for each layer (Figure 27) show that saprock (289 ppb) and saprolite (342 ppb) are enriched compared to bedrock (174 ppb). Residual clay (145 ppb) is depleted compared to saprolite and saprock. The ferruginous residual clay has significantly less Au (36 ppb mean), much the same as the sand and gravel (28 ppb and 27 ppb, respectively). This is much lower than observed at the Argo deposit and Argo palaeochannel (Sections 5.1 and 5.2) where the sand and gravel units are primarily at the palaeochannel base. The sand and gravel units at Apollo tend to occur as small pockets (Figure 26) close to the residual regolith at much higher elevation and might not be of high significance. Moderately high Au concentrations were observed in the lower lake clay (84 ppb) and lignite (132 ppb). Gold content then decreases steadily upwards to 48 ppb in the alluvium.

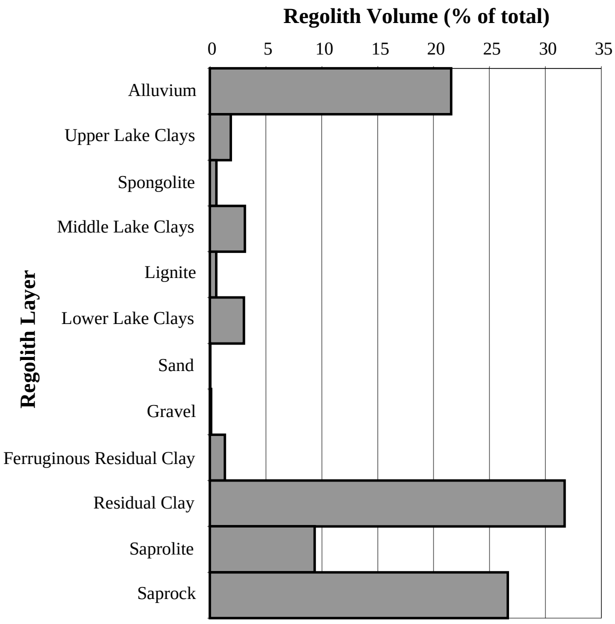

Figure 26: Comparative volume of each regolith layer from the Apollo deposit, as a percentage of total regolith volume.

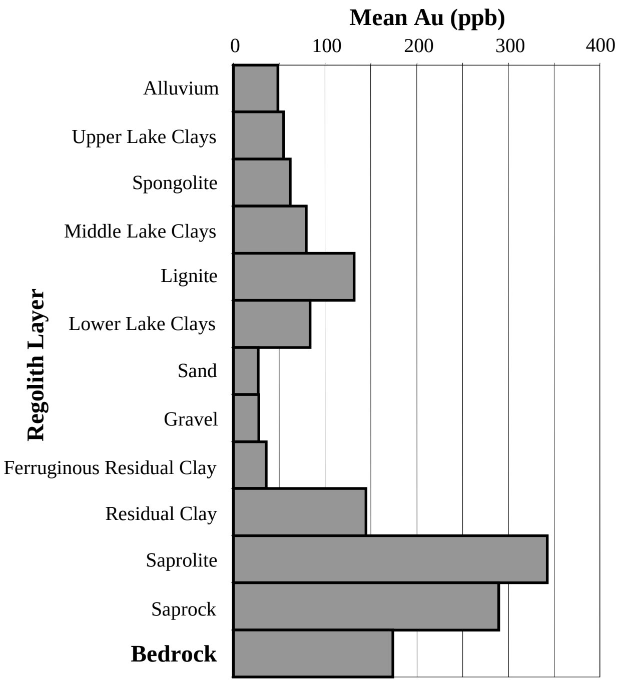

Figure 27: Mean Au for each regolith layer and bedrock from the Apollo deposit.

Further calculations of mean Au at the Apollo deposit were based on 3 m thick horizontal slices taken above and below the weathering front, the pedoplasmation front (saprolite/residual clay interface), and the unconformity. The reliability of the results of each slice has been calculated using the method described in Section 2.4. As with the slices from the Argo palaeochannel, only those slices considered 60% reliable or greater were used.

Calculations of mean Au as a function of distance from the weathering front (Figure 28) show that Au concentrations in the bedrock vary from a minimum of 128 ppb 36-33 m below the weathering front to a maximum just below the weathering front of 246 ppb. Concentrations continue to increase to a maximum value of 325 ppb 12-15 m above the weathering front, and then decreases upwards.

Figure 29 shows mean Au as a function of distance from the pedoplasmation front. Limited data indicate that the Au distribution is reasonably homogenous below the front and in the 3 m above (range 274 -310 ppb). It then appears to decrease up-profile.

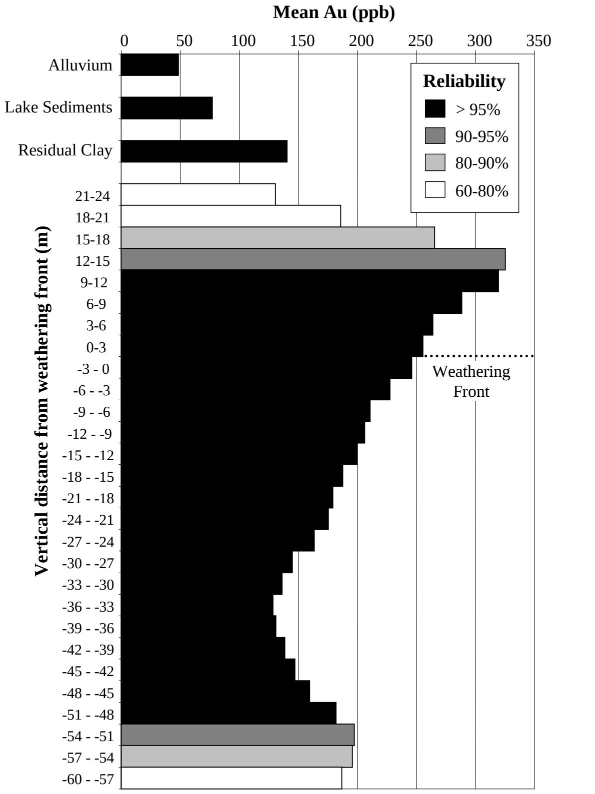

Figure 28: Mean Au vs depth from the weathering front at the Apollo deposit.

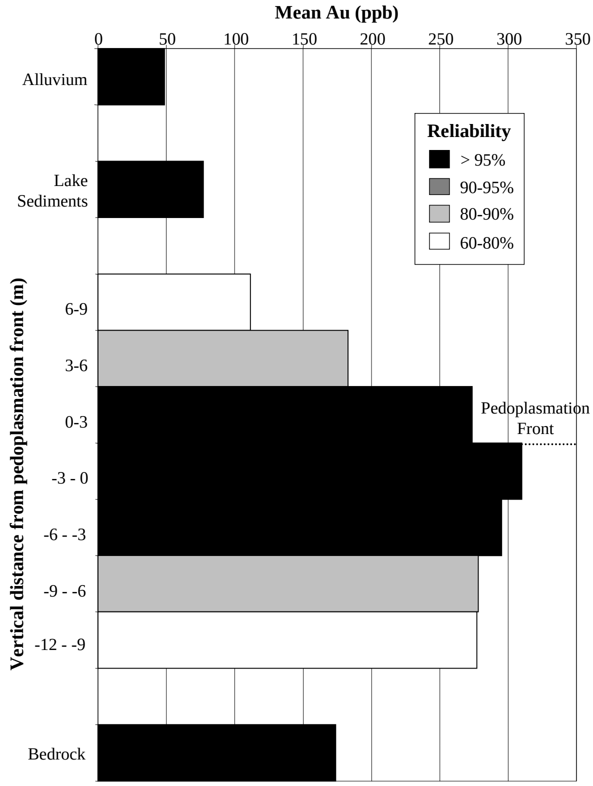

Figure 29: Mean Au vs depth from the pedoplasmation front at the Apollo deposit.

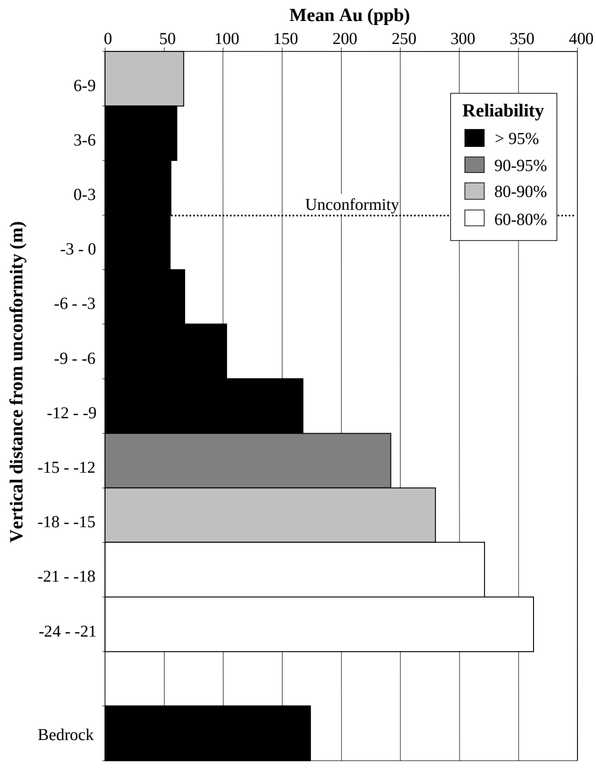

Figure 30: Mean Au vs depth from the unconformity at the Apollo deposit.

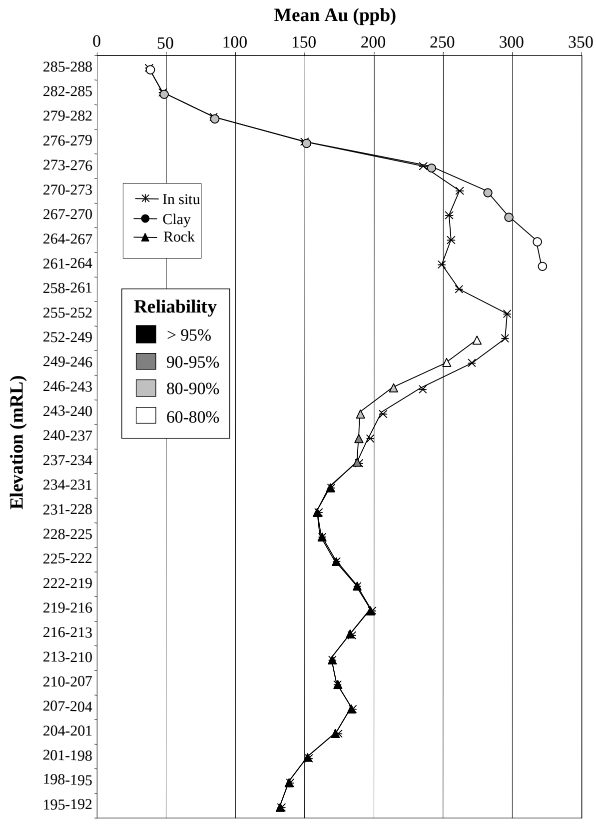

Figure 31: Mean Au vs depth for all residual regolith at the Apollo deposit.

Figure 30 shows mean Au as a function of distance from the unconformity. Gold concentration is greatest at depth (363 ppb, 21-24 m below the unconformity) and steadily decreases upwards towards the unconformity (approximately 55 ppb). Concentrations then remain fairly homogenous upwards for at least 9 m above the unconformity.

Calculations of Au concentration in the residual regolith as a function of depth are shown in Figure 31. There is little variation in most of the bedrock, but a significant increase occurs at about 240-243 mRL. Gold content appears to continue to increase upwards in the residual regolith, peaking at 321 ppb at about 261-264 mRL. At about 270-273 mRL (281 ppb) a sharp decrease begins and only 15 m above, the concentration is 37 ppb, marking the depletion zone (Section 4.3.3). Comparison with Table 5 suggests that this depletion, though strong, is less than that observed at Argo.

5.4 DISCUSSION

The residual clay layer has the greatest mass of all the residual regolith units at the Argo and Apollo deposits, with the exception of areas around the base of the palaeochannel where this unit may have been eroded (Figure 11). Ferruginous residual clay is also insignificant in the Argo palaeochannel, comprising less than 0.1% of the total regolith mass (Figure 20).

The Au depletion zone present above approximately 270-276 mRL in the Argo and Apollo residual regolith (Figure 31, Table 5) does not appear in the palaeochannel sediments (Figure 25). It is possible that depletion occurred prior to Eocene sedimentation, but it is also possible that the sediments may never have contained sufficient Au to be significantly affected by a later event. It is well known, elsewhere in the region, that depletion is generally associated with salinity related to post-Miocene aridity (Gedeon and Butt, 1990).

There is less sediment in the northern part of the Apollo deposit, as would be expected in a former upland area. The gravel, sand, lignite and spongolite total less than 1% and can be regarded as insignificant (Figure 26). Alluvium forms a large proportion of the regolith over both the Argo and Apollo deposits (15% and 22%, Figures 18 and 26, respectively).

Calculated Au abundance at both deposits show that Au is enriched in the saprock and further again in the saprolite compared to bedrock (Figures 18 and 26). The Au concentrations then decrease significantly in the residual clay and further still in the ferruginous residual clay.

The residual profile in the Argo channel has somewhat different Au distribution than the area as a whole (Figure 21). Gold concentration is lower in the saprock and saprolite than in the bedrock but increases in the residual and ferruginous residual clays, presumably reflecting enrichment in these units low in the landscape and below the depletion zone. The highest mean Au content in the palaeochannel and over the greater area of the Argo deposit is in the basal gravel layer at the unconformity. The sand unit overlying the gravel also contains significant Au which then decrease up-profile, with the lowest values in the spongolite. The upper lake clays have slightly higher Au concentration than the spongolite, but slightly less than the middle lake clays. Gold content then decreases further in the uppermost alluvium layer.

The differences in Au concentration in the transported units at the Apollo deposit (Figure 27) are probably due to these units making up a very small amount of the total regolith mass (< 1%) and occurring as small pockets of material in uplands. Thus, the apparent enrichment in the lignite and depletion in the ferruginous residual clay, sand and gravel compared to the surrounding lake clays may have little or no significance.

The Au concentration calculations as a function of depth at the Argo channel (Figure 25) are in broad agreement with the patterns illustrated by the regolith layers (Figure 21). Reliable Au content calculations for the bedrock and residual regolith are limited but show the same decrease in the lower residual profile and increase in the upper residual profile (Figure 23). Reliable data for the transported units are more comprehensive and show the same peak at the unconformity followed by a steady decrease up-profile (Figure 24).

Data for Au concentration within bedrock at Apollo show some variation, with a major increase just below the weathering front (Figure 31). This is possibly due to primary variation in the ore body or, alternatively, as the bedrock slices get closer to the recognized saprock there may be some weathering influence and supergene enrichment.

Within the weathered residual material at Apollo (Figure 31), there appears to be strong enrichment of Au in the saprock and saprolite, culminating at a peak just below 270 m elevation. This corresponds to about 9-15 m above the weathering front (Figure 28) or within 3 m of either side of the saprolite/residual clay boundary (Figure 29). Above this elevation, Au concentration decreases significantly from 321 to 37 ppb.

6 CONCLUSIONS

The computer program MVS has successfully been used for the three-dimensional visualization of stratigraphy and Au geochemistry at the Argo and Apollo deposits. The program was also used to calculate Au concentrations in the different regolith units and the variation in Au content with elevation or distance from a regolith transition.

Using logging provided by WMC Resources Ltd, the residual profile was divided into bedrock, saprock, saprolite, residual clay and ferruginous residual clay. The overlying sediments were split into basal gravels and sands, lignite, spongolite, lake clays between these units and overlying alluvium. This stratigraphy is broadly similar to that in previous studies.

The weathering front shows a broad deepening below the palaeochannel as well as two narrow chasms along the strike of the two deposits. Of the major *in situ* units (saprock, saprolite and residual clay), the residual clay is generally thickest, but it, the saprolite, and, in places, the saprock, are truncated directly beneath the palaeochannel. There is also a thin ferruginous clay unit that is mostly confined to the upland areas and hill flanks of the pre-Eocene topography.

At the Argo and Apollo deposits, Au concentrations of greater than 1 ppm in the bedrock become supergene-enriched blankets in the saprock, saprolite and lower residual clay, with a major Au depletion above 270 - 276 mRL elevation. The depletion appears to be of the order of 60 - 80% at Apollo and greater than 90% at Argo.

The basal gravel and, to a lesser extent, sand horizons of the palaeochannel are strongly enriched in Au. This could be due to detrital accumulation of Au or to dispersion from underlying moderate mineralization, or both. Above these horizons, there is a smooth reduction in Au concentration upwards through the palaeochannel sediments, with the exception of spongolite, which is particularly low in Au. The previously suggested association of Au with lignite in the palaeochannel is not observed, but instead appears related to proximity to the unconformity. High Au concentrations observed at surface are postulated to be mainly cross-hole contamination.

ACKNOWLEDGEMENTS

The authors acknowledge the assistance of WMC Resources Ltd., with particular thanks to Ms M. Carey for the provision of the database for the area, advice during the investigation and field assistance. M. Skwarnecki and C.R.M. Butt provided advice during the final production of this report.

REFERENCES

Butt, C.R.M., Gray, D.J., Robertson, I.D.M., Lintern, M.J., Anand, R.R., Britt, A.F., Bristow, A.P.J., Munday, M.J., Phang, C., Smith, R.E. and Wildman, J.E., 1997. Geochemical exploration in areas of transported overburden, Yilgarn Craton and environs, Western Australia. CRC LEME Restricted Report 36R, 150 pp.

Carey, M.L. and Dusci, M.E., 1999. WMC Resources exploration successes in lake terrains – applications of element dispersion, Kambalda, WA. In: Pain, C.F. (Editor), New Approaches to an Old Continent, Regolith '98 Proceedings, p135-148. Cooperative Research Centre for Landscape Evolution and Mineral Exploration, Perth, 341 pp.

Clarke, J.D.A., 1994a. Evolution of the Lefroy and Cowan palaeodrainage channels, Western Australia. Australian Journal of Earth Sciences, 41:55-68.

Clarke, J.D.A., 1994b. Geomorphology of the Kambalda region, Western Australia. Australian Journal of Earth Sciences, 41:229-239.

Clarke, J.D.A., 1994c. Lake Lefroy, a palaeodrainage playa in Western Australia. Australian Journal of Earth Sciences, 41:417-427.

Clarke, J.D.A., Bone, Y. and James, N.P., 1994. Marine incursions into palaeodrainages at Kambalda and Norseman, Western Australia. 12th Australian Geological Convention, Geological Society of Australia, Abstracts, 37:63-64.

Gedeon, A.Z. and Butt, C.R.M., 1990. Morphology and geochemistry of particulate gold in the lateritic regolith, Mystery Zone, Mt Percy, Kalgoorlie, Western Australia. CSIRO Division of Exploration Geoscience, Perth, Restricted Report Number 124R, 45 pp. Republished 1998 as CRC LEME Open File Report 23.

Lintern, M.J., Craig, M.A. and Carver, R.N, 1997. Geochemical studies of the soil and vegetation at the Apollo gold deposit, Kambalda, Western Australia. CRC LEME Restricted Report 30R, 23 pp.

Lintern, M.J. and Gray, D.J., 1995. Progress statement for the Kalgoorlie study area – Argo deposit, Western Australia. CSIRO Exploration & Mining Report 96R, 22 pp.

Woolrich, N.K., 1994. The stratigraphy and gold mineralisation of the Argo tertiary palaeochannel at Kambalda, Western Australia. Honours thesis, Curtin University of Technology, 101 pp and appendices (unpublished).

Zheng, H., Wyrwoll, K.-H., Li, Z. and Powell, C. McA., 1998. Onset of aridity in southern Western Australia – a preliminary palaeomagnetic appraisal. Global and Planetary Change, 18:175-187.

APPENDIX 1 ENCLOSED CD

A1.1 FOLDER: ARGO 3D AU

This folder contains the Microsoft PowerPoint file “Argo3DAu.ppt” containing 15 slides depicting three-dimensional images of the Au distribution at the Argo deposit.

Slide:	**Depicts:**
1.	Au distribution with 30 ppb cut-off, looking NE
2.	Au distribution with 30 ppb cut-off, looking SE
3.	Au distribution with 30 ppb cut-off, looking SW
4.	Au distribution with 30 ppb cut-off, looking NW
5.	Au distribution with 100 ppb cut-off, looking SE
6.	Au distribution with 100 ppb cut-off, looking NW
7.	Au distribution with 100 ppb cut-off, looking WSW
8.	Au distribution with 100 ppb cut-off, looking ENE
9.	Au distribution with 300 ppb cut-off, looking ENE
10.	Au distribution with 300 ppb cut-off, looking NW
11.	Au distribution with 300 ppb cut-off, looking WSW
12.	Au distribution with 1 ppm cut-off, looking ENE
13.	Au distribution with 1 ppm cut-off, looking SE
14.	Au distribution with 1 ppm cut-off, looking SW
15.	Au distribution with 1 ppm cut-off, looking NW

A1.2 FOLDER: ARGO AU SURFACES

This folder contains plan and oblique views of the Au distribution at each regolith surface at the Argo deposit.

File:	**Depicts:**
Feresclay.bmp	Au distribution on the upper surface of the Fe-rich residual clay layer, looking NW
Feresclay_plan.bmp	Au distribution on the upper surface of the Fe-rich residual clay layer, plan view
gravel.bmp	Au distribution on the upper surface of the gravel layer, looking NW
gravel_plan.bmp	Au distribution on the upper surface of the gravel layer, plan view
lignite.bmp	Au distribution on the upper surface of the lignite layer, looking NW
lignite_plan.bmp	Au distribution on the upper surface of the lignite layer, plan view
llakeclay.bmp	Au distribution on the upper surface of the lower lake clays, looking NW
llakeclay_plan.bmp	Au distribution on the upper surface of the lower lake clays, plan view
mlakeclay.bmp	Au distribution on the upper surface of the middle lake clays, looking NW
mlakeclay_plan.bmp	Au distribution on the upper surface of the middle lake clays, plan view
resclay.bmp	Au distribution on the upper surface of the residual clay layer, looking NW
resclay_plan.bmp	Au distribution on the upper surface of the residual clay layer, plan view
rock.bmp	Au distribution on the upper surface of the bedrock, looking NW
rock_plan.bmp	Au distribution on the upper surface of the bedrock, plan view
sand.bmp	Au distribution on the upper surface of the sand layer, looking NW
sand_plan.bmp	Au distribution on the upper surface of the sand layer, plan view
saprock.bmp	Au distribution on the upper surface of the saprock layer, looking NW
saprock_plan.bmp	Au distribution on the upper surface of the saprock layer, plan view
saprolite.bmp	Au distribution on the upper surface of the saprolite layer, looking NW
saprolite_plan.bmp	Au distribution on the upper surface of the saprolite layer, plan view
spongolite.bmp	Au distribution on the upper surface of the spongolite layer, looking NW
spongolite_plan.bmp	Au distribution on the upper surface of the spongolite layer, plan view
surface.bmp	Au distribution on the ground surface, looking NW

surface_plan.bmp	Au distribution on the ground surface, plan view
ulakeclay.bmp	Au distribution on the upper surface of the upper lake clays, looking NW
ulakeclay_plan.bmp	Au distribution on the upper surface of the upper lake clays, plan view

A1.3 FOLDER: ARGO AU X-SECTIONS

This folder contains the Microsoft PowerPoint file "Argo Au X-Sections.ppt" containing 30 slides depicting two-dimensional cross sections of the Au distribution at the Argo deposit.

Slide	**Depicts:**
1.	Au distribution along a north-south transect at 383400 mE
2.	Au distribution along a north-south transect at 383450 mE
3.	Au distribution along a north-south transect at 383500 mE
4.	Au distribution along a north-south transect at 383550 mE
5.	Au distribution along a north-south transect at 383560 mE
6.	Au distribution along a north-south transect at 383570 mE
7.	Au distribution along a north-south transect at 383580 mE
8.	Au distribution along a north-south transect at 383590 mE
9.	Au distribution along a north-south transect at 383600 mE
10.	Au distribution along a north-south transect at 383605 mE
11.	Au distribution along a north-south transect at 383610 mE
12.	Au distribution along a north-south transect at 383615 mE
13.	Au distribution along a north-south transect at 383620 mE
14.	Au distribution along a north-south transect at 383625 mE
15.	Au distribution along a north-south transect at 383630 mE
16.	Au distribution along a north-south transect at 383635 mE
17.	Au distribution along a north-south transect at 383640 mE
18.	Au distribution along a north-south transect at 383645 mE
19.	Au distribution along a north-south transect at 383650 mE
20.	Au distribution along a north-south transect at 383660 mE
21.	Au distribution along a north-south transect at 383665 mE
22.	Au distribution along a north-south transect at 383670 mE
23.	Au distribution along a north-south transect at 383675 mE
24.	Au distribution along a north-south transect at 383680 mE
25.	Au distribution along a north-south transect at 383690 mE
26.	Au distribution along a north-south transect at 383700 mE
27.	Au distribution along a north-south transect at 383710 mE
28.	Au distribution along a north-south transect at 383720 mE
29.	Au distribution along a north-south transect at 383750 mE
30.	Au distribution along a north-south transect at 383800 mE

A1.4 FOLDER: ARGO REGOLITH

This folder contains three-dimensional diagrams of the regolith at the Argo deposit.

File:	**Depicts:**
allA_expl.bmp	All layers, exploded, looking NW
allA_tog.bmp	All layers, together, looking NW
allB_expl.bmp	All layers, exploded, looking NE
allB_tog.bmp	All layers, together, looking NE
FeresclayA_expl.bmp	Regolith profile to the top of the Fe-rich residual clay, exploded, looking NW

FeresclayA_tog.bmp	Regolith profile to the top of the Fe-rich residual clay, together, looking NW
FeresclayB_expl.bmp	Regolith profile to the top of the Fe-rich residual clay, exploded, looking NE
FeresclayB_tog.bmp	Regolith profile to the top of the Fe-rich residual clay, together, looking NE
gravelA_expl.bmp	Regolith profile to the top of the gravel layer, exploded, looking NW
gravelA_tog.bmp	Regolith profile to the top of the gravel layer, together, looking NW
gravelB_expl.bmp	Regolith profile to the top of the gravel layer, exploded, looking NE
gravelB_tog.bmp	Regolith profile to the top of the gravel layer, together, looking NE
ligniteA_expl.bmp	Regolith profile to the top of the lignite layer, exploded, looking NW
ligniteA_tog.bmp	Regolith profile to the top of the lignite layer, together, looking NW
ligniteB_expl.bmp	Regolith profile to the top of the lignite layer, exploded, looking NE
ligniteB_tog.bmp	Regolith profile to the top of the lignite layer, together, looking NE
llakeclayA_expl.bmp	Regolith profile to the top of the lower lake clays, exploded, looking NW
llakeclayA_tog.bmp	Regolith profile to the top of the lower lake clays, together, looking NW
llakeclayB_expl.bmp	Regolith profile to the top of the lower lake clays, exploded, looking NE
llakeclayB_tog.bmp	Regolith profile to the top of the lower lake clays, together, looking NE
mlakeclayA_expl.bmp	Regolith profile to the top of the middle lake clays, exploded, looking NW
mlakeclayA_tog.bmp	Regolith profile to the top of the middle lake clays, together, looking NW
mlakeclayB_expl.bmp	Regolith profile to the top of the middle lake clays, exploded, looking NW
mlakeclayB_tog.bmp	Regolith profile to the top of the middle lake clays, together, looking NW
resclayA_expl.bmp	Regolith profile to the top of the residual clay, exploded, looking NW
resclayA_tog.bmp	Regolith profile to the top of the residual clay, together, looking NW
resclayB_expl.bmp	Regolith profile to the top of the residual clay, exploded, looking NE
resclayB_tog.bmp	Regolith profile to the top of the residual clay, together, looking NE
rockA.bmp	Bedrock, looking NW
rockB.bmp	Bedrock, looking SE
sandA_expl.bmp	Regolith profile to the top of the sand layer, exploded, looking NW
sandA_tog.bmp	Regolith profile to the top of the sand layer, together, looking NW
sandB_expl.bmp	Regolith profile to the top of the sand layer, exploded, looking NE
sandB_tog.bmp	Regolith profile to the top of the sand layer, together, looking NE
saprockA_expl.bmp	Regolith profile to the top of saprock, exploded, looking NW
saprockA_tog.bmp	Regolith profile to the top of saprock, together, looking NW
saprockB_expl.bmp	Regolith profile to the top of saprock, exploded, looking NE
saprockB_tog.bmp	Regolith profile to the top of saprock, together, looking NE
saproliteA_expl.bmp	Regolith profile to the top of saprolite, exploded, looking NW
saproliteA_tog.bmp	Regolith profile to the top of saprolite, together, looking NW
saproliteB_expl.bmp	Regolith profile to the top of saprolite, exploded, looking NE
saproliteB_tog.bmp	Regolith profile to the top of saprolite, together, looking NE
spongoliteA_expl.bmp	Regolith profile to the top of the spongolite layer, exploded, looking NW
spongoliteA_tog.bmp	Regolith profile to the top of the spongolite layer, together, looking NW
spongoliteB_expl.bmp	Regolith profile to the top of the spongolite layer, exploded, looking NE
spongoliteB_tog.bmp	Regolith profile to the top of the spongolite layer, together, looking NE
ulakeclayA_expl.bmp	Regolith profile to the top of the upper lake clays, exploded, looking NW
ulakeclayA_tog.bmp	Regolith profile to the top of the upper lake clays, together, looking NW
ulakeclayB_expl.bmp	Regolith profile to the top of the upper lake clays, exploded, looking NE
ulakeclayB_tog.bmp	Regolith profile to the top of the upper lake clays, together, looking NE

A1.5 FOLDER: ARGO-APOLLO AU SURFACES

This folder contains plan and oblique views of the Au distribution at the interface of each regolith unit at the Argo and Apollo deposits.

File:	Depicts:
FeresclayA.bmp	Au distribution at the Fe-rich residual clay/gravel interface, looking NW
FeresclayB.bmp	Au distribution at the Fe-rich residual clay/gravel interface, looking NE
Feresclay_plan.bmp	Au distribution at the Fe-rich residual clay/gravel interface, plan view
gravelA.bmp	Au distribution at the gravel/sand interface, looking NW
gravelB.bmp	Au distribution at the gravel/sand interface, looking NE
gravel_plan.bmp	Au distribution at the gravel/sand interface, plan view
ligniteA.bmp	Au distribution at the lignite/middle lake clays interface, looking NW
ligniteB.bmp	Au distribution at the lignite/middle lake clays interface, looking NE
lignite_plan.bmp	Au distribution at the lignite/middle lake clays interface, plan view
llakeclayA.bmp	Au distribution at the lower lake clays/lignite interface, looking NW
llakeclayB.bmp	Au distribution at the lower lake clays/lignite interface, looking NE
llakeclay_plan.bmp	Au distribution at the lower lake clays/lignite interface, plan view
mlakeclayA.bmp	Au distribution at the middle lake clays/spongolite interface, looking NW
mlakeclayB.bmp	Au distribution at the middle lake clays/spongolite interface, looking NE
mlakeclay_plan.bmp	Au distribution at the middle lake clays/spongolite interface, plan view
resclayA.bmp	Au distribution at the residual clay/ferruginous residual clay interface, looking NW
resclayB.bmp	Au distribution at the residual clay/ferruginous residual clay interface, looking NE
resclay_plan.bmp	Au distribution at the residual clay/ferruginous residual clay interface, plan view
rockA.bmp	Au distribution at the bedrock/saprock interface, looking NW
rockB.bmp	Au distribution at the bedrock/saprock interface, looking NE
rock_plan.bmp	Au distribution at the bedrock/saprock interface, plan view
sandA.bmp	Au distribution at the sand/lower lake clays interface, looking NW
sandB.bmp	Au distribution at the sand/lower lake clays interface, looking NE
sand_plan.bmp	Au distribution at the sand/lower lake clays interface, plan view
saprockA.bmp	Au distribution at the saprock/saprolite interface, looking NW
saprockB.bmp	Au distribution at the saprock/saprolite interface, looking NE
saprock_plan.bmp	Au distribution at the saprock/saprolite interface, plan view
saproliteA.bmp	Au distribution at the saprolite/residual clay interface, looking NW
saproliteB.bmp	Au distribution at the saprolite/residual clay interface, looking NE
saprolite_plan.bmp	Au distribution at the saprolite/residual clay interface, plan view
spongoliteA.bmp	Au distribution at the spongolite/upper lake clays interface, looking NW
spongoliteB.bmp	Au distribution at the spongolite/upper lake clays interface, looking NE
spongolite_plan.bmp	Au distribution at the spongolite/upper lake clays interface, plan view
surfaceA.bmp	Au distribution at the surface, looking NW
surfaceB.bmp	Au distribution at the surface, looking NE
surface_plan.bmp	Au distribution at the surface, plan view
ulakeclayA.bmp	Au distribution at the upper lake clays/alluvium interface, looking NW
ulakeclayB.bmp	Au distribution at the upper lake clays/alluvium interface, looking NE
ulakeclay_plan.bmp	Au distribution at the upper lake clays/alluvium interface, plan view

A1.6 FOLDER: ARGO-APOLLO REGOLITH

This folder contains the Microsoft PowerPoint file "ArgoApolloRegolith.ppt" containing 50 slides depicting the regolith stratigraphy of the area surrounding the Argo and Apollo deposits.

Slide:	Depicts:
1.	All layers, looking NE
2.	All layers, looking NW
3.	Top of upper lake clays, looking NE
4.	Top of upper lake clays, looking NW
5.	Top of spongolite, looking NE
6.	Top of spongolite, looking NW
7.	Top of middle lake clays, looking NE
8.	Top of middle lake clays, looking NW
9.	Top of lignite, looking NE
10.	Top of lignite, looking NW
11.	Top of lower lake clays, looking NE
12.	Top of lower lake clays, looking NW
13.	Top of sand, looking NE
14.	Top of sand, looking NW
15.	Top of gravel, looking NE
16.	Top of gravel, looking NW
17.	Top of ferruginous residual clay, looking NE
18.	Top of ferruginous residual clay, looking NW
19.	Top of residual clay, looking NE
20.	Top of residual clay, looking NW
21.	Top of saprolite, looking NE
22.	Top of saprolite, looking NW
23.	Top of saprock, looking NE
24.	Top of saprock, looking NW
25.	Top of bedrock, looking NE
26.	Top of bedrock, looking NW
27.	All layers, exploded, looking NE
28.	All layers, exploded, looking NW
29.	Top of upper lake clays, exploded, looking NE
30.	Top of upper lake clays, exploded, looking NW
31.	Top of spongolite, exploded, looking NE
32.	Top of spongolite, exploded, looking NW
33.	Top of middle lake clays, exploded, looking NE
34.	Top of middle lake clays, exploded, looking NW
35.	Top of lignite, exploded, looking NE
36.	Top of lignite, exploded, looking NW
37.	Top of lower lake clays, exploded, looking NE
38.	Top of lower lake clays, exploded, looking NW
39.	Top of sand, exploded, looking NE
40.	Top of sand, exploded, looking NW
41.	Top of gravel, exploded, looking NE
42.	Top of gravel, exploded, looking NW
43.	Top of ferruginous residual clay, exploded, looking NE
44.	Top of ferruginous residual clay, exploded, looking NW
45.	Top of residual clay, exploded, looking NE
46.	Top of residual clay, exploded, looking NW
47.	Top of saprolite, exploded, looking NE
48.	Top of saprolite, exploded, looking NW
49.	Top of saprock, exploded, looking NE
50.	Top of saprock, exploded, looking NW

A1.7 FOLDER: REGIONAL AU SURFACES

This folder contains plan and oblique views of the Au distribution at the interface of each regolith unit across the Argo and Apollo region.

File:	**Depicts:**
FeresclayA.bmp	Au distribution at the Fe-rich residual clay/gravel interface, looking NW
FeresclayB.bmp	Au distribution at the Fe-rich residual clay/gravel interface, looking NE
Feresclay_plan.bmp	Au distribution at the Fe-rich residual clay/gravel interface, plan view
gravelA.bmp	Au distribution at the gravel/sand interface, looking NW
gravelB.bmp	Au distribution at the gravel/sand interface, looking NE
gravel_plan.bmp	Au distribution at the gravel/sand interface, plan view
ligniteA.bmp	Au distribution at the lignite/middle lake clays interface, looking NW
ligniteB.bmp	Au distribution at the lignite/middle lake clays interface, looking NE
lignite_plan.bmp	Au distribution at the lignite/middle lake clays interface, plan view
llakeclayA.bmp	Au distribution at the lower lake clays/lignite interface, looking NW
llakeclayB.bmp	Au distribution at the lower lake clays/lignite interface, looking NE
llakeclay_plan.bmp	Au distribution at the lower lake clays/lignite interface, plan view
mlakeclayA.bmp	Au distribution at the middle lake clays/spongolite interface, looking NW
mlakeclayB.bmp	Au distribution at the middle lake clays/spongolite interface, looking NE
mlakeclay_plan.bmp	Au distribution at the middle lake clays/spongolite interface, plan view
resclayA.bmp	Au distribution at the residual clay/ferruginous residual clay interface, looking NW
resclayB.bmp	Au distribution at the residual clay/ferruginous residual clay interface, looking NE
resclay_plan.bmp	Au distribution at the residual clay/ferruginous residual clay interface, plan view
rockA.bmp	Au distribution at the bedrock/saprock interface, looking NW
rockB.bmp	Au distribution at the bedrock/saprock interface, looking NE
rock_plan.bmp	Au distribution at the bedrock/saprock interface, plan view
sandA.bmp	Au distribution at the sand/lower lake clays interface, looking NW
sandB.bmp	Au distribution at the sand/lower lake clays interface, looking NE
sand_plan.bmp	Au distribution at the sand/lower lake clays interface, plan view
saprockA.bmp	Au distribution at the saprock/saprolite interface, looking NW
saprockB.bmp	Au distribution at the saprock/saprolite interface, looking NE
saprock_plan.bmp	Au distribution at the saprock/saprolite interface, plan view
saproliteA.bmp	Au distribution at the saprolite/residual clay interface, looking NW
saproliteB.bmp	Au distribution at the saprolite/residual clay interface, looking NE
saprolite_plan.bmp	Au distribution at the saprolite/residual clay interface, plan view
spongoliteA.bmp	Au distribution at the spongolite/upper lake clays interface, looking NW
spongoliteB.bmp	Au distribution at the spongolite/upper lake clays interface, looking NE
spongolite_plan.bmp	Au distribution at the spongolite/upper lake clays interface, plan view
surfaceA.bmp	Au distribution at the surface, looking NW
surfaceB.bmp	Au distribution at the surface, looking NE
surface_plan.bmp	Au distribution at the surface, plan view
ulakeclayA.bmp	Au distribution at the upper lake clays/alluvium interface, looking NW
ulakeclayB.bmp	Au distribution at the upper lake clays/alluvium interface, looking NE
ulakeclay_plan.bmp	Au distribution at the upper lake clays/alluvium interface, plan view

A1.8 FOLDER: REGIONAL AU X-SECTIONS

This folder contains the Microsoft PowerPoint file "Regional Au X-Sections.ppt" containing 23 slides depicting two-dimensional cross sections of the Au distribution across the Argo and Apollo Au deposits. Refer to Figure A1.1 for section locations.

Slide:	Depicts:
1.	Au distribution along a north-south transect at 383615 mE
2.	Au distribution along a north-south transect at 383665 mE
3.	Au distribution over cross section A1, approximately along strike of the palaeochannel
4.	Au distribution over cross section A, approximately along strike of the palaeochannel
5.	Au distribution over cross section A, approximately along strike of the palaeochannel, residual profile only
6.	Au distribution over cross section B, approximately along strike of the palaeochannel
7.	Au distribution over cross section B, approximately along strike of the palaeochannel, residual profile only
8.	Au distribution over cross section C, cross-cutting the palaeochannel
9.	Au distribution over cross section C, cross-cutting the palaeochannel, residual profile only
10.	Au distribution over cross section D, cross-cutting the palaeochannel
11.	Au distribution over cross section D, cross-cutting the palaeochannel, residual profile only
12.	Au distribution over cross section E, cross-cutting the palaeochannel
13.	Au distribution over cross section E, cross-cutting the palaeochannel, residual profile only
14.	Au distribution over cross section F, cross-cutting the palaeochannel
15.	Au distribution over cross section F, cross-cutting the palaeochannel, residual profile only
16.	Au distribution over cross section G, cross-cutting the palaeochannel
17.	Au distribution over cross section G, cross-cutting the palaeochannel, residual profile only
18.	Au distribution over cross section H, cross-cutting the palaeochannel
19.	Au distribution over cross section H, cross-cutting the palaeochannel, residual profile only
20.	Au distribution over cross section I, cross-cutting the palaeochannel
21.	Au distribution over cross section I, cross-cutting the palaeochannel, residual profile only
22.	Au distribution over cross section J, cross-cutting the palaeochannel
23.	Au distribution over cross section J, cross-cutting the palaeochannel, residual profile only

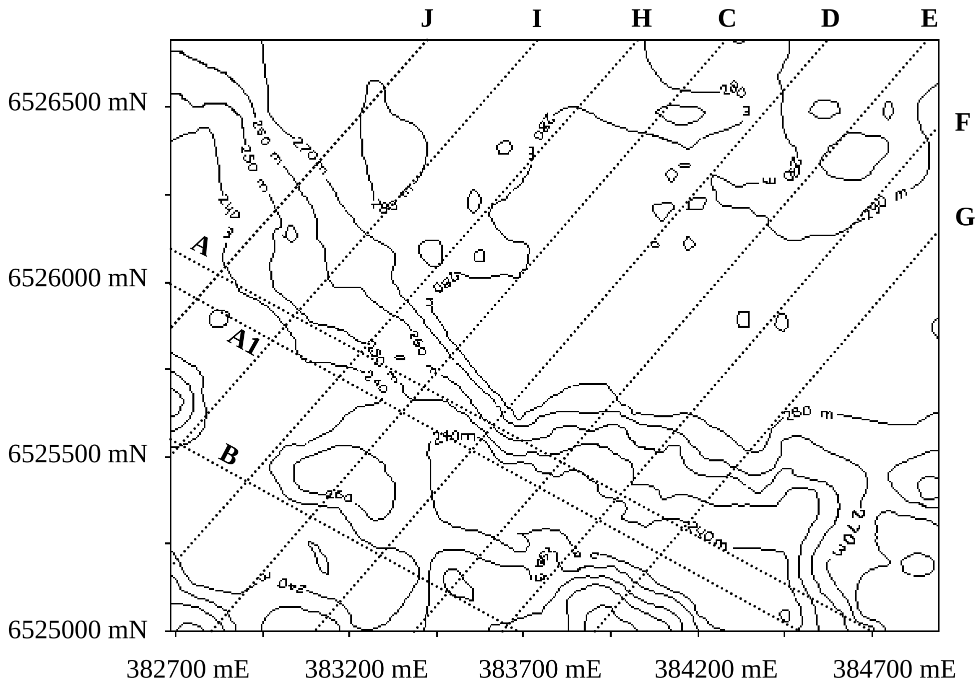

Figure A1.1 Transects (A-J) across the Argo-Apollo region showing the locations of the two-dimensional regolith and gold distribution cross-sections. The map shows the surface of the residual regolith with elevation in mRL (see Figure 11).

A1.9 FOLDER: REGIONAL REGOLITH X-SECTIONS

This folder contains cross sections of the regional regolith stratigraphy around the Argo and Apollo Au deposits. Refer to Figure A1.1 for section locations.

File:	**Depicts:**
sectionA.bmp	Regolith stratigraphy over cross section A, approximately along strike of the palaeochannel
sectionB.bmp	Regolith stratigraphy over cross section B, approximately along strike of the palaeochannel
sectionC.bmp	Regolith stratigraphy over cross section C, cross-cutting the palaeochannel
sectionD.bmp	Regolith stratigraphy over cross section D, cross-cutting the palaeochannel
sectionE.bmp	Regolith stratigraphy over cross section E, cross-cutting the palaeochannel
sectionF.bmp	Regolith stratigraphy over cross section F, cross-cutting the palaeochannel
sectionG.bmp	Regolith stratigraphy over cross section G, cross-cutting the palaeochannel
sectionH.bmp	Regolith stratigraphy over cross section H, cross-cutting the palaeochannel
sectionI.bmp	Regolith stratigraphy over cross section I, cross-cutting the palaeochannel
sectionJ.bmp	Regolith stratigraphy over cross section J, cross-cutting the palaeochannel

APPENDIX 2 GOLD CONCENTRATION CALCULATIONS

A2.1 DATA FOR THE ARGO DEPOSIT

Argo deposit, Regolith Layers (see Figures 18 & 19)			
All Layers:			
Layer	**“Mass” (1 x 10^6 kg)**	**% of total Regolith Volume**	**Mean Au (ppb)**
Alluvium	7612.00	14.82	54.23
Upper Lake Clays	5318.00	10.35	79.13
Spongolite	1768.00	3.44	30.84
Middle Lake Clays	5053.00	9.84	101.35
Lignite	2075.00	4.04	147.81
Lower Lake Clays	3216.00	6.26	185.91
Sand	2534.00	4.93	649.57
Gravel	219.50	0.43	1534.85
Fe-rich Residual Clay	616.40	1.20	114.97
Residual Clay	10450.00	20.34	298.28
Saprolite	5962.00	11.61	541.76
Saprock	6546.00	12.74	402.54
Rock	40610.00		260.77
Regolith Total	**51369.90**		
All	**91979.90**	**100.00**	**260.17**
Grouped Layers:			
Layer	**“Mass” (1 x 10^6 kg)**	**% of total Regolith Volume**	**Mean Au (ppb)**
Alluvium	7612.00	14.82	54.23
Other Lake Sediments	17430.00	33.93	108.55
Sand/Gravel	2753.50	5.36	720.14
Residual Clay	11066.40	21.54	288.07
Saprock/Saprolite	12508.00	24.35	468.90
Rock	40610.00		260.77
Regolith Total	**51369.90**		
All	**91979.90**	**100.00**	**260.17**

“Mass” is a nominal value based on volume (see Section 2.4).

A2.2 DATA FOR THE ARGO CHANNEL

Argo Channel, Regolith Layers (see Figures 20 & 21)			
All Layers:			
Layer	**"Mass" (1 x 10^6 kg)**	**% of total Regolith Volume**	**Mean Au (ppb)**
Alluvium	2890.00	12.37	39.10
Upper Lake Clays	3540.00	15.15	100.30
Spongolite	1630.00	6.97	29.80
Middle Lake Clays	3180.00	13.61	132.80
Lignite	1500.00	6.42	167.70
Lower Lake Clays	1730.00	7.40	287.20
Sand	2470.00	10.57	651.60
Gravel	205.00	0.88	1635.90
Fe-rich Residual Clay	16.30	0.07	1245.40
Residual Clay	1480.00	6.33	949.20
Saprolite	2200.00	9.41	705.80
Saprock	2530.00	10.83	472.90
Rock	7730.00		735.70
Regolith Total	**23371.30**		
All	**31101.30**	**100.00**	**433.85**
Grouped Layers:			
Layer	**"Mass" (1 x 10^6 kg)**	**% of total Regolith Volume**	**Mean Au (ppb)**
Alluvium	2890.00	12.4	39.10
Other Lake Sediments	11580.00	49.5	135.95
Sand/Gravel	2675.00	11.4	727.03
Residual Clay	1496.30	6.4	952.43
Saprock/Saprolite	4730.00	20.2	581.23
Rock	7730.00		735.70
Regolith Total	**23371.30**		
All	**31101.30**	**100.00**	**433.85**

"Mass" is a nominal value based on volume (see Section 2.4).

Argo Channel, Transported Material (see Figure 24)							
Slice (Elevation mRL)	**"Mass" (1 x 10^6 kg)**	**Reliability (%)**	**Mean Au (ppb)**	**Slice (Elevation mRL)**	**"Mass" (1 x 10^6 kg)**	**Reliability (%)**	**Mean Au (ppb)**
297 - 297.95	1.05	0.11	12.20	**261 - 264**	**883.00**	**92.75**	**177.00**
294 - 297	392.00	41.18	37.60	**258 - 261**	**865.00**	**90.86**	**178.20**
291 - 294	**930.00**	**97.69**	**45.30**	**255 - 258**	**850.00**	**89.29**	**188.00**
288 - 291	**943.00**	**99.05**	**53.60**	**252 - 255**	**825.00**	**86.66**	**210.30**
285 - 288	**942.00**	**98.95**	**63.50**	**249 - 252**	**800.00**	**84.03**	**252.80**
282 - 285	**941.00**	**98.84**	**68.20**	**246 - 249**	**777.00**	**81.62**	**317.70**
279 - 282	**951.00**	**99.89**	**73.50**	**243 - 246**	**762.00**	**80.04**	**430.50**
276 - 279	**952.00**	**100.00**	**79.20**	**240 - 243**	**694.00**	**72.90**	**573.20**
273 - 276	**949.00**	**99.68**	**100.20**	**237 - 240**	**538.00**	**56.51**	**925.50**
270 - 273	**941.00**	**98.84**	**114.20**	234 - 237	289.00	30.36	1533.60
267 - 270	**924.00**	**97.06**	**130.90**	231 - 234	17.30	1.82	1264.30
264 - 267	**904.00**	**94.96**	**161.70**	228 - 231	1.08	0.11	581.00
				Max. Value	**952.00**	**100.00**	**1533.60**

Bold type denotes those slices with a reliability greater or equal to 60% (see Section 2.4)
"Mass" is a nominal value based on volume (see Section 2.4).

Argo Channel, Residual Regolith (see Figure 23)							
Slice (Elevation mRL)	**"Mass" (1 x 10^6 kg)**	**Reliability (%)**	**Mean Au (ppb)**	**Slice (Elevation mRL)**	**"Mass" (1 x 10^6 kg)**	**Reliability (%)**	**Mean Au (ppb)**
276 - 279	0.16	0.02	93.00	237 - 240	359.00	43.57	555.10
273 - 276	1.11	0.13	204.60	**234 - 237**	**585.00**	**71.00**	**895.60**
270 - 273	5.44	0.66	257.30	**231 - 234**	**824.00**	**100.00**	**1097.90**
267 - 270	19.10	2.32	473.70	**228 - 231**	**771.00**	**93.57**	**769.00**
264 - 267	36.60	4.44	937.90	**225 - 228**	**682.00**	**82.77**	**525.80**
261 - 264	52.70	6.40	1535.80	**222 - 225**	**594.00**	**72.09**	**430.60**
258 - 261	68.40	8.30	1781.20	**219 - 222**	**509.00**	**61.77**	**380.80**
255 - 258	84.90	10.30	1537.10	216 - 219	420.00	50.97	334.80
252 - 255	101.00	12.26	1110.40	213 - 216	260.00	31.55	210.90
249 - 252	117.00	14.20	926.40	210 - 213	148.00	17.96	174.20
246 - 249	125.00	15.17	810.40	207 - 210	48.60	5.90	171.20
243 - 246	137.00	16.63	641.70	204 - 207	7.09	0.86	144.70
240 - 243	212.00	25.73	532.50				
				Max Value	**824.00**	**100.00**	**1781.20**

Bold type denotes those slices with a reliability greater or equal to 60% (see Section 2.4)
"Mass" is a nominal value based on volume (see Section 2.4).

Argo Channel, Bedrock (see Figure 22)							
Slice (Elevation mRL)	**"Mass" (1 x 10^6 kg)**	**Reliability (%)**	**Mean Au (ppb)**	**Slice (Elevation mRL)**	**"Mass" (1 x 10^6 kg)**	**Reliability (%)**	**Mean Au (ppb)**
255 - 257	0.17	0.02	5705.20	222 - 225	336.00	38.89	667.20
252 - 255	2.21	0.26	3212.90	219 - 222	410.00	47.45	805.20
249 - 252	6.33	0.73	2069.20	216 - 219	488.00	56.48	818.50
246 - 249	16.70	1.93	1259.50	**213 - 216**	**644.00**	**74.54**	**688.90**
243 - 246	27.20	3.15	1101.70	**210 - 213**	**744.00**	**86.11**	**621.80**
240 - 243	38.20	4.42	1188.40	**207 - 210**	**827.00**	**95.72**	**666.70**
237 - 240	53.00	6.13	1564.60	**204 - 207**	**864.00**	**100.00**	**706.40**
234 - 237	75.60	8.75	1679.50	**201 - 204**	**864.00**	**100.00**	**736.20**
231 - 234	107.00	12.38	1340.80	**198 - 201**	**864.00**	**100.00**	**722.20**
228 - 231	173.00	20.02	883.60	**195 - 198**	**864.00**	**100.00**	**697.00**
225 - 228	253.00	29.28	675.10				
				Max. Value	**864.00**	**100.00**	**5705.20**

Bold type denotes those slices with a reliability greater or equal to 60% (see Section 2.4)
"Mass" is a nominal value based on volume (see Section 2.4).

Argo Channel, Bedrock & Residual Regolith (combined) (see Figure 25)							
Slice (Elevation mRL)	**"Mass" (1 x 10^6 kg)**	**Reliability (%)**	**Mean Au (ppb)**	**Slice (Elevation mRL)**	**"Mass" (1 x 10^6 kg)**	**Reliability (%)**	**Mean Au (ppb)**
276 - 279	0.16	0.02	92.90	**234 - 237**	**661.00**	**70.02**	**985.20**
273 - 276	1.11	0.12	204.70	**231 - 234**	**932.00**	**98.73**	**1125.80**
270 - 273	5.44	0.58	257.30	**228 - 231**	**944.00**	**100.00**	**789.90**
267 - 270	19.10	2.02	473.70	**225 - 228**	**944.00**	**100.00**	**566.20**
264 - 267	36.60	3.88	937.90	**222 - 225**	**944.00**	**100.00**	**516.10**
261 - 264	52.70	5.58	1535.80	**219 - 222**	**944.00**	**100.00**	**570.00**
258 - 261	68.40	7.25	1781.20	**216 - 219**	**944.00**	**100.00**	**594.80**
255 - 258	85.10	9.01	1544.60	**213 - 216**	**944.00**	**100.00**	**551.40**
252 - 255	103.00	10.91	1155.80	**210 - 213**	**944.00**	**100.00**	**547.60**
249 - 252	123.00	13.03	985.40	**207 - 210**	**944.00**	**100.00**	**639.20**
246 - 249	141.00	14.94	863.30	**204 - 207**	**944.00**	**100.00**	**701.80**
243 - 246	164.00	17.37	717.80	**201 - 204**	**944.00**	**100.00**	**736.20**
240 - 243	250.00	26.48	632.70	**198 - 201**	**944.00**	**100.00**	**722.20**
237 - 240	412.00	43.64	684.90	**195 - 198**	**944.00**	**100.00**	**697.00**
				Max. Value	**944.00**	**100.00**	**1781.20**

Bold type denotes those slices with a reliability greater or equal to 60% (see Section 2.4)
"Mass" is a nominal value based on volume (see Section 2.4).

A2.3 DATA FOR THE APOLLO DEPOSIT

Apollo deposit, Regolith Layers (see Figures 26 & 27)			
All Layers:			
Layer	**"Mass" (1 x 10^6 kg)**	**% of total Regolith Volume**	**Mean Au (ppb)**
Alluvium	5303.00	21.58	48.46
Upper Lake Clays	455.30	1.85	54.56
Spongolite	147.10	0.60	62.01
Middle Lake Clays	765.10	3.11	79.39
Lignite	140.80	0.57	131.53
Lower Lake Clays	748.60	3.05	83.90
Sand	16.00	0.07	26.88
Gravel	27.56	0.11	27.77
Fe-rich Residual Clay	328.00	1.34	35.70
Residual Clay	7792.00	31.72	144.76
Saprolite	2299.00	9.36	342.28
Saprock	6546.00	26.64	289.49
Rock	32270.00		173.88
Regolith Total	**24568.46**		
All	**56838.46**	**100.00**	**173.59**
Grouped Layers:			
Layer	**"Mass" (1 x 10^6 kg)**	**% of total Regolith Volume**	**Mean Au ppb)**
Alluvium	5303.00	21.58	48.46
Lake Sediments	2300.46	9.36	77.04
Residual Clay	8120.00	33.05	140.36
Saprock/Saprolite	8845.00	36.00	303.21
Rock	32270.00		173.88
Regolith Total	**24568.46**		
All	**56838.46**	**100.00**	**173.59**

"Mass" is a nominal value based on volume (see Section 2.4).

Apollo deposit, Pedoplasmation Front (see Figure 29)							
Slice (m from front)	**“Mass” (1 x 10^6 kg)**	**Reliability (%)**	**Mean Au (ppb)**	**Slice (m from front)**	**“Mass” (1 x 10^6 kg)**	**Reliability (%)**	**Mean Au (ppb)**
42-45	5.21	0.28	20.40	**-12 - -9**	**1359.00**	**73.06**	**277.19**
39-42	15.85	0.85	20.54	-15 - -12	926.20	49.80	273.38
36-39	27.13	1.46	21.36	-18 - -15	521.20	28.02	304.68
33-36	40.06	2.15	22.98	-21 - -18	283.20	15.23	360.17
30-33	54.77	2.94	26.00	-24 - -21	166.30	8.94	460.19
27-30	93.61	5.03	33.31	-27 - -24	97.16	5.22	569.27
24-27	164.20	8.83	38.99	-30 - -27	50.09	2.69	678.58
21-24	259.70	13.96	41.86	-33 - -30	20.35	1.09	890.91
18-21	368.40	19.81	45.44	-36 - -33	10.88	0.58	931.07
15-18	513.10	27.59	52.56	-39 - -36	6.635	0.36	918.01
12-15	708.10	38.07	61.80	-42 - -39	4.35	0.23	999.31
9-12	1015.00	54.57	81.36	-45 - -42	2.97	0.16	1206.41
6-9	**1390.00**	**74.73**	**111.58**	-48 - -45	2.05	0.11	1557.02
3-6	**1623.00**	**87.26**	**182.93**	-51 - -48	1.37	0.07	1546.65
0-3	**1806.00**	**97.10**	**273.75**	-54 - -51	0.84	0.04	1237.30
-3 - 0	**1860.00**	**100.00**	**310.00**	-57 - -54	0.44	0.02	706.87
-6 - -3	**1823.00**	**98.01**	**295.23**	-60 - -57	0.14	0.01	352.43
-9 - -6	**1669.00**	**89.73**	**278.19**				
				Max. Value	**1860.00**	**100.00**	**1557.02**

Bold type denotes those slices with a reliability greater or equal to 60% (see Section 2.4)
“Mass” is a nominal value based on volume (see Section 2.4).

Apollo deposit, Unconformity (see Figure 30)							
Slice (m from uncon.)	**“Mass” (1 x 10^6 kg)**	**Reliability (%)**	**Mean Au (ppb)**	**Slice (m from uncon.)**	**“Mass” (1 x 10^6 kg)**	**Reliability (%)**	**Mean Au (ppb)**
30-33	8.19	0.44	20.68	**-24 - -21**	**1261.00**	**67.25**	**362.73**
27-30	70.92	3.78	29.51	-27 - -24	1071.00	57.12	391.97
24-27	166.60	8.89	31.43	-30 - -27	813.10	43.37	420.86
21-24	244.40	13.03	34.64	-33 - -30	609.30	32.50	383.72
18-21	302.00	16.11	40.40	-36 - -33	439.30	23.43	297.75
15-18	355.40	18.95	47.89	-39 - -36	257.90	13.75	319.27
12-15	429.80	22.92	55.61	-42 - -39	136.30	7.27	380.56
9-12	686.00	36.59	60.29	-45 - -42	87.06	4.64	354.81
6-9	**1591.00**	**84.85**	**66.56**	-48 - -45	57.38	3.06	292.96
3-6	**1875.00**	**100.00**	**60.80**	-51 - -48	37.06	1.98	233.05
0-3	**1868.00**	**99.63**	**55.62**	-54 - -51	23.85	1.27	211.28
-3 - 0	**1860.00**	**99.20**	**55.00**	-57 - -54	13.75	0.73	267.35
-6 - -3	**1857.00**	**99.04**	**67.42**	-60 - -57	4.14	0.22	694.78
-9 - -6	**1850.00**	**98.67**	**102.86**	-63 - -60	1.49	0.08	1405.89
-12 - -9	**1807.00**	**96.37**	**167.63**	-66 - -63	0.87	0.05	1299.07
-15 - -12	**1718.00**	**91.63**	**241.97**	-69 - -66	0.45	0.02	934.44
-18 - -15	**1573.00**	**83.89**	**279.78**	-72 - -69	0.12	0.01	473.56
-21 - -18	**1410.00**	**75.20**	**321.21**				
				Max. Value	**1875.00**	**100.00**	**1405.89**

Bold type denotes those slices with a reliability greater or equal to 60% (see Section 2.4)
“Mass” is a nominal value based on volume (see Section 2.4).

Apollo deposit, Weathering Front (see Figure 28)							
Slice (m from front)	**"Mass" (1×10^6 kg)**	**Reliability (%)**	**Mean Au (ppb)**	**Slice (m from front)**	**"Mass" (1×10^6 kg)**	**Reliability (%)**	**Mean Au (ppb)**
57-60	0.45	0.02	20.22	**-15 - -12**	**1781.00**	**92.52**	**199.61**
54-57	7.07	0.37	20.45	**-18 - -15**	**1758.00**	**91.32**	**187.49**
51-54	15.29	0.79	20.67	**-21 - -18**	**1723.00**	**89.51**	**178.93**
48-51	25.12	1.30	21.82	**-24 - -21**	**1675.00**	**87.01**	**175.22**
45-48	38.50	2.00	25.34	**-27 - -24**	**1629.00**	**84.62**	**163.29**
42-45	56.78	2.95	30.10	**-30 - -27**	**1588.00**	**82.49**	**144.71**
39-42	93.48	4.86	34.56	**-33 - -30**	**1546.00**	**80.31**	**136.09**
36-39	195.90	10.18	42.83	**-36 - -33**	**1499.00**	**77.87**	**128.35**
33-36	375.60	19.51	50.61	**-39 - -36**	**1442.00**	**74.91**	**130.72**
30-33	545.90	28.36	61.42	**-42 - -39**	**1380.00**	**71.69**	**138.62**
27-30	751.10	39.02	74.18	**-45 - -42**	**1338.00**	**69.51**	**146.94**
24-27	1029.00	53.45	94.38	**-48 - -45**	**1288.00**	**66.91**	**159.47**
21-24	**1251.00**	**64.99**	**130.46**	**-51 - -48**	**1216.00**	**63.17**	**181.74**
18-21	**1438.00**	**74.70**	**185.74**	-54 - -51	1115.00	57.92	197.13
15-18	**1631.00**	**84.73**	**265.05**	-57 - -54	944.40	49.06	195.68
12-15	**1789.00**	**92.94**	**324.93**	-60 - -57	731.80	38.02	186.80
9-12	**1890.00**	**98.18**	**319.26**	-63 - -60	560.20	29.10	175.17
6-9	**1925.00**	**100.00**	**288.21**	-66 - -63	421.80	21.91	159.48
3-6	**1918.00**	**99.64**	**263.76**	-69 - -66	276.20	14.35	141.42
0-3	**1905.00**	**98.96**	**255.22**	-72 - -69	182.60	9.49	108.76
-3 - 0	**1868.00**	**97.04**	**245.82**	-75 - -72	97.95	5.09	72.27
-6 - -3	**1855.00**	**96.36**	**227.44**	-78 - -75	29.79	1.55	49.88
-9 - -6	**1835.00**	**95.32**	**210.68**	-81 - -78	3.66	0.19	23.42
-12 - -9	**1807.00**	**93.87**	**206.03**				
				Max. Value	**1925.00**	**100.00**	**324.93**

Bold type denotes those slices with a reliability greater or equal to 60% (see Section 2.4)
"Mass" is a nominal value based on volume (see Section 2.4).

Apollo deposit, Residual Regolith (see Figure 31)							
Slice (Elevation mRL)	**"Mass" (1 x 10^6 kg)**	**Reliability (%)**	**Mean Au (ppb)**	**Slice (Elevation mRL)**	**"Mass" (1 x 10^6 kg)**	**Reliability (%)**	**Mean Au (ppb)**
291-294	0.69	0.04	26.64	252-249	647.52	37.72	326.20
288-291	222.40	12.38	36.71	249-246	443.03	25.94	324.90
285-288	**1085.37**	**60.42**	**37.31**	246-243	276.88	16.23	342.63
282-285	**1451.10**	**80.77**	**47.34**	243-240	184.30	10.88	335.11
279-282	**1523.50**	**84.80**	**83.93**	240-237	132.43	7.88	283.47
276-279	**1568.50**	**87.31**	**150.23**	237-234	91.19	5.41	194.77
273-276	**1591.90**	**88.61**	**240.53**	234-231	54.470	3.22	145.42
270-273	**1581.60**	**88.04**	**281.11**	231-228	29.370	1.76	167.38
267-270	**1496.00**	**83.27**	**296.26**	228-225	14.90	0.91	259.53
264-267	**1391.20**	**76.80**	**316.85**	225-222	4.57	0.29	550.62
261-264	**1233.30**	**68.62**	**320.56**	222-219	1.04	0.07	1171.46
258-261	1020.80	57.65	339.61	219-216	0.52	0.03	843.06
255-252	846.40	48.54	354.44	216-213	0.17	0.01	298.28
				Max. Value	**1581.60**	**88.04**	**1171.46**

Bold type denotes those slices with a reliability greater or equal to 60% (see Section 2.4)
"Mass" is a nominal value based on volume (see Section 2.4).

Apollo deposit, Bedrock & Residual Regolith (combined) (see Figure 31)							
Slice (Elevation mRL)	**"Mass" (1 x 10^6 kg)**	**Reliability (%)**	**Mean Au (ppb)**	**Slice (Elevation mRL)**	**"Mass" (1 x 10^6 kg)**	**Reliability (%)**	**Mean Au (ppb)**
291-294	0.69	0.04	26.64	**240-237**	**1680.43**	**92.77**	**196.22**
288-291	222.40	12.28	36.71	**237-234**	**1685.19**	**93.03**	**187.97**
285-288	**1085.37**	**59.92**	**37.31**	**234-231**	**1693.47**	**93.49**	**168.01**
282-285	**1451.10**	**80.11**	**47.34**	**231-228**	**1668.37**	**92.10**	**158.79**
279-282	**1524.08**	**84.14**	**83.91**	**228-225**	**1628.90**	**89.92**	**161.56**
276-279	**1577.50**	**87.09**	**149.70**	**225-222**	**1591.57**	**87.86**	**171.85**
273-276	**1638.88**	**90.48**	**235.43**	**222-219**	**1549.04**	**85.52**	**186.97**
270-273	**1727.30**	**95.36**	**261.73**	**219-216**	**1495.52**	**82.56**	**197.48**
267-270	**1796.50**	**99.18**	**254.14**	**216-213**	**1437.17**	**79.34**	**182.96**
264-267	**1811.40**	**100.00**	**255.49**	**213-210**	**1390.00**	**76.74**	**168.85**
261-264	**1797.30**	**99.22**	**248.82**	**210-207**	**1355.00**	**74.80**	**172.55**
258-261	**1770.60**	**97.75**	**261.31**	**207-204**	**1332.00**	**73.53**	**183.48**
255-252	**1743.80**	**96.27**	**295.96**	**204-201**	**1307.00**	**72.15**	**172.92**
252-249	**1716.52**	**94.76**	**294.44**	**201-198**	**1291.00**	**71.27**	**151.82**
249-246	**1708.03**	**94.29**	**270.51**	**198-195**	**1264.00**	**69.78**	**138.29**
246-243	**1705.88**	**94.17**	**234.05**	**195-192**	**1224.00**	**67.57**	**131.94**
243-240	**1693.30**	**93.48**	**205.37**				
				Max. Value	**1811.40**	**100.00**	**295.96**

Bold type denotes those slices with a reliability greater or equal to 60% (see Section 2.4)
"Mass" is a nominal value based on volume (see Section 2.4).

A2.4 DATA FOR THE RESIDUAL REGOLITH DEPLETION ZONE (see Table 5)

		ARGO		ARGO CHANNEL		APOLLO	
		"Mass" (1 x 10^6 kg)	Mean Au (ppb)	"Mass" (1 x 10^6 kg)	Mean Au (ppb)	"Mass" (1 x 10^6 kg)	Mean Au (ppb)
Ferruginous Residual Clay	All	615.70	111.13	16.26	1245.39	328.00	35.70
	>270 m	575.60	51.58	3.18	221.55	324.80	35.56
	<270 m	40.03	967.27	13.09	1491.22	3.20	54.27
	>270 m/<270 m Ratio (%)	93.5	5.3	19.5	14.9	99.0	65.5
	>276 m	494.00	36.68	0.15	93.00	314.60	34.81
	<276 m	121.70	412.41	16.09	1254.82	13.41	56.57
	>270 m/<270 m Ratio (%)	80.2	8.9	0.9	7.4	95.9	61.5
Residual Clay	All	10430.00	300.48	1476.00	949.19	7792.00	144.76
	>270 m	4991.00	91.75	3.58	264.65	5837.00	128.42
	<270 m	5430.00	492.45	1472.00	950.41	1951.00	193.70
	>270 m/<270 m Ratio (%)	47.9	18.6	0.2	27.8	74.9	66.3
	>276 m	2683.00	47.52	5584	91.85	4505.00	84.00
	<276 m	7739.00	388.42	1476.00	949.19	3282.00	228.61
	>270 m/<270 m Ratio (%)	25.7	12.2	0	9.7	57.9	36.7
Saprolite	All	5950.00	541.85	2199.00	705.78	2299.00	342.28
	>270 m	340.30	167.41	0	-	834.50	267.71
	<270 m	5607.00	564.65	2199.00	705.78	1464.00	384.08
	>270 m/<270 m Ratio (%)	5.7	29.6	0	-	36.3	69.7
	>276 m	49.12	52.28	0	-	366.60	84.23
	<276 m	5900.00	545.93	2199.00	705.78	1932.00	391.67
	>270 m/<270 m Ratio (%)	0.8	9.6	0	-	16.0	21.5
Saprock	All	6484.00	413.48	2527.00	472.89	6546.00	289.49
	>270 m	139.60	72.56	0	-	2063.00	156.47
	<270 m	6343.00	421.09	2527.00	472.89	4475.00	351.29
	>270 m/<270 m Ratio (%)	2.2	17.2	0	-	31.6	44.5
	>276 m	2.53	28.36	0	--	685.00	87.71
	<276 m	6481.00	413.67	2527.00	472.89	5857.00	313.13
	>270 m/<270 m Ratio (%)	0.04	6.9	0	-	10.5	28.0

"Mass" is a nominal value based on volume (see Section 2.4).

APPENDIX 3 INTERACTIVE 3D IMAGES

A3.1 INSTRUCTIONS FOR VIEWING VRMLS

Appendix 3 consists of folder "Appendix3-interactive" on the enclosed CD. It contains:

- A web page – "ARGO.htm" and an associated images folder.
- A folder called "VRML" which contains VRMLs (files written with Virtual Reality Modelling Language). These are 3D images that the user can manipulate and view from different angles.
- An installation file for Cosmo Player.

You will need to have a web browser installed on your computer (but it does not have to be connected to an outside line). You will need a plug-in, such as COSMO Player, that will enable your internet browser to display the VRMLs. To install Cosmo Player from this CD, follow the steps below (which are also set out on the web page).

Note: The computer will need at least 200 Mhz and 64 MB to run the VRMLs effectively.

Instructions

1. Open the CD, then open the "Appendix3-interactive" folder. Click on the icon named "cosmo_win95nt_eng.exe" and it will launch with prompts. Read the first page, close any open Windows programs, then click NEXT.
2. Agree to the License Agreement and click YES.
3. It will determine which internet browsers are on your system and list some options. Choose the option that you usually use, e.g. Netscape Communicator 4.5 or Internet Explorer (provided with Windows). Some users will have older systems and will need to choose "Other". Click NEXT.
4. Choose the destination folder using the BROWSE button. Then click NEXT. The plug-in will now install itself.
5. It will then ask you if you would like to associate all VRML related files (.wrl, .wrz, .wrl.gz) with Cosmo Player. Choose YES.
6. Set up is complete. You should be able click on the options below and use the VRMLs.

Web Page
A web page is provided as a convenient way of navigating through the VRMLs. In particular, it provides a handy reference to the regolith legend and geochemical scale as these features are not supported by the VRMLs.

Either open the page through your browser (File Menu – Open Page) or if your computer is configured to recongise htm/html files then just click on the "ARGO.htm" icon to launch the page.

The following VRMLs are provided:

A3.2 ARGO AND APOLLO REGOLITH

WMC logging enabled CRC LEME to distinguish 13 regolith units at the Argo and Apollo Deposits, seven of which are able to presented interactively. Note: Some of these files are very large and may load slowly.

File:	**Depicts:**
sand.wrl	Regolith profile to the top of sand
gravel.wrl	Regolith profile to the top of gravel
Feresclay.wrl	Regolith profile to the top of ferruginous residual clay
resclay.wrl	Regolith profile to the top of residual clay
saprolite.wrl	Regolith profile to the top of saprolite
saprock.wrl	Regolith profile to the top of saprock
bedrock.wrl	Bedrock

A3.3 ARGO AND APOLLO AU CONCENTRATIONS

CRC LEME generated 3D models of the Au concentrations along the upper surface of each regolith layer. The data was filtered so that the minimum Au value was set to 10 ppb and the maximum to 1 ppm. Thus all values of 10 ppb or lower are at the cool end of the colour scale (blue) and values of 1 ppm or greater are displayed at the hot end (red).

File:	**Depicts:**
surfacechem.wrl	Au distribution along the surface (top of alluvium)
ulakeclaychem.wrl	Au distribution along the upper lake clay/alluvium interface
spongolitechem.wrl	Au distribution along the spongolite/upper lake clay interface
mlakeclaychem.wrl	Au distribution along the middle lake clays/spongolite interface
lignitechem.wrl	Au distribution along the lignite/middle lake clays interface
llakeclaychem.wrl	Au distribution along the lower lake clays/lignite interface
sandchem.wrl	Au distribution along the sand/lower lake clays interface
gravelchem.wrl	Au distribution along the gravel/sand interface
Feresclaychem.wrl	Au distribution along the ferruginous residual clay/gravel interface (unconformity)
resclaychem.wrl	Au distribution along the residual clay/ferruginous residual clay interface
saprolitechem.wrl	Au distribution along the saprolite/residual clay interface
saprockchem.wrl	Au distribution along the saprock/saprolite interface
bedrockchem.wrl	Au distribution along the bedrock/saprock interface (base of weathering)

A3.4 ARGO 3D AU CUT-OFFS

These VRMLs depict three-dimensional models of Au distribution at the Argo deposit. The colours match the regolith legend and show all those parts of each regolith layer that have, for example, 300 ppb Au concentration or greater.

File:	**Depicts:**
argo300ppb.wrl	Au distribution with 300 ppb cut-off
argo1ppm.wrl	Au distribution with 1 ppm cut-off